

Università degli Studi di Padova



Facoltà di Ingegneria

Dipartimento di Tecnica e Gestione dei Sistemi Industriali

Laurea Magistrale in Ingegneria dell'Innovazione del Prodotto

Anno Accademico 2010-2011

Structural properties of Ge- and Hf-doped multicrystalline silicon

Relatore: ***Ch.mo Prof. FRANCO BONOLLO***

Correlatore: ***Prof. LARS ARNBERG***

Laureando: ***Gianmaria Minozzi***



Norwegian University of
Science and Technology

Affidavit

The work of this thesis has been conducted at the Department of Materials Science and Engineering at the Norwegian University of Science and Technology (NTNU) from 22th February 2010 to 2nd July 2010.

I confirm that I have performed this thesis “Structural properties of Ge- and Hf-doped multicrystalline silicon” independently, i.e. without illegal help of others and without other sources than the mentioned ones. Acquired thoughts from other sources, directly or indirectly, are marked as those.

Trondheim, July 2010.

Gianmaria Minozzi

Acknowledgement

First of all I want to thank Prof. Lars Arnberg who made possible the course of my internship abroad. Thank you for all support you gave me during my stay, for working with you in a really nice group, for taking time to discuss and to read my thesis. Thank you also for giving me the opportunity to take part at the meeting in Oppdal, where the work was enlivened with enjoyable activities.

I thank Prof. Franco Bonollo to giving me the chance to take part at the exchange study period in Norway.

I thank Martin P. Bellmann as well for giving me all the theoretical background needed, for taking time to discuss results and issues, to read and correct my thesis and to give me the right advices to write it in the best way. Thank you also for giving me the opportunity to participate at the Renewable Energy Research Conference in Trondheim with a poster presentation. I want to apologise to him if my performances on Mondays were not so good: it was due to the so-called “Erasmus weekends”.

I thank Chiara Modanese for training on polishing and on the FTIR. Thank you also for being “a big Italian help”.

Last but not least I want to thank my parents and my sister for supporting me wholeheartedly at any time: only a few words to say that without them this work and these long years of study would not have been possible.

Abstract

Presently the efficiency of standard solar cells made from multi-crystalline silicon (mc-Si) reaches values in the range of 16%. A main point for the achievement of higher cell efficiencies is a significant improvement of the bulk material. Of particular relevance are extended defects such as dislocations, which are important recombination centres. Therefore the reduction of the overall dislocation density should improve the performance of the material.

Previous results have shown that the dislocations nucleate and multiply during crystal growth due to local stresses which arise from differences in the local thermal expansion. Especially, the formation of localised areas with very high dislocation density (up to 10^8 cm^{-2}) are crucial because these regions are particularly detrimental for the charge carrier lifetime and the material performance. A further improvement of multi-crystalline materials requires a substantial reduction of these bad regions.

The goal of the present investigation is to reduce the dislocation density by hindering the nucleation and motion of dislocations. Solid solution hardening by impurities, which cause local strain, is a well known phenomenon in metals. Since germanium and hafnium are electrically inactive elements with high local strain in silicon due to the larger size, their effect on dislocations has been studied here.

We have investigated different mc-Si materials which were intentionally doped with germanium concentrations up to 1% of weight and hafnium concentrations of 6 and 11% of weight. The influence of germanium and hafnium on the distribution of oxygen and carbon was studied by Fourier Transform Infrared Spectroscopy (FTIR). The grain size was measured with the Intercept method, the resistivity of the sample with a four-point probe and the dislocation density with laser scanning equipment (PV-Scan).

Extended abstract

Celle solari: stato dell'arte

Le celle solari in silicio sono state il traino dell'industria fotovoltaica per molti anni e tuttora rappresentano l'80% dell'intera produzione mondiale. I moduli fotovoltaici costruiti con questo tipo di celle hanno una grande affidabilità e garanzie di durata che arrivano a 20 o 25 anni, dato eccezionale per qualsiasi prodotto manifatturiero. Nonostante celle di diversi materiali continuino ad essere sviluppate e prodotte, sarà difficile spodestare il silicio da questa posizione. La tecnologia che sta alla base è quella dell'elettronica dei semiconduttori: una cella solare in silicio è una particolare forma di diodo a semiconduttore. Fortunatamente, il silicio in forma di quarzo (diossido di silicio) è un componente molto comune dell'intera crosta terrestre ed è essenzialmente non tossico. Ci sono due tipi principali di celle solari di silicio cristallino attualmente prodotti in elevati volumi:

- *Monocristallino.* Il tipo più efficiente, costituito da un wafer molto sottile ricavato da un cristallo di silicio puro. I wafer circolari di circa 15 cm di diametro hanno una struttura cristallina ordinata con proprietà uniformi e prevedibili. Tuttavia, richiedono processi di produzione attenti e costosi, incluso il drogaggio con piccole quantità di elementi per arrivare alle caratteristiche elettriche richieste. L'efficienza dei moduli di silicio monocristallino in commercio è dell'ordine del 14-16%. La superficie di moduli necessaria è di circa $7 \text{ m}^2/\text{kW}_\text{p}$.
- *Policristallino.* Questo tipo di cella è prodotto attraverso processi industriali di fusione. Quando il silicio fuso si raffredda, dà vita ad un lingotto con struttura policristallina irregolare che viene successivamente tagliato in fette sottili e quadrate per creare le singole celle. La loro struttura cristallina, essendo casuale, porta ad avere efficienze leggermente inferiori al silicio monocristallino, ma questo svantaggio è compensato dal costo inferiore del wafer. L'efficienza di un modulo in silicio policristallino è nell'ordine del 11-15%. La superficie necessaria è di circa $8 \text{ m}^2/\text{kW}_\text{p}$.

Le celle create in laboratorio raggiungono efficienze maggiori rispetto a quelle prodotte industrialmente in elevati volumi. L'efficienza dei moduli è leggermente minore rispetto a quella di una singola cella perché la superficie di un modulo non può essere completamente ricoperta dalle celle ed anche il telaio occupa una parte importante di superficie. È sempre

importante distinguere tra l'efficienza della cella e l'efficienza del modulo.

È presente anche un altro tipo di cella solare in silicio comunemente in uso:

- *Amorfo*. Le celle solari in silicio amorfio sono più economiche delle celle solari in silicio cristallino, ma hanno un'efficienza molto minore: circa il 6-8%. Oggi vengono usate tipicamente nelle facciate degli edifici e la superficie richiesta è di circa 16 $\text{m}^2/\text{kW}_\text{p}$.

La tecnologia che sta alla base delle celle solari in silicio cristallino è ormai consolidata ed è spesso chiamata di “prima generazione”: di questa fanno parte tutte le celle che si vedono sulle case, sulle industrie e sugli edifici commerciali. Tuttavia, è importante sapere che altri materiali semiconduttori possono essere utilizzati per produrre celle solari. La maggior parte di questi ricade sotto il nome di *film sottile* ed implica il deposito di uno strato molto sottile di semiconduttore su una varietà di substrati. I prodotti a film sottile sono generalmente considerati come l'ultimo obiettivo per il fotovoltaico terrestre in quanto utilizzano quantità molto ridotte di semiconduttore e processi continui su larga scala che non implicano il taglio e il montaggio di singoli wafer. I moduli a film sottile basati su composti di semiconduttori quali *rame-indio-selenio* (*CIS*) e *cadmio-tellurio* (*CdTe*) vengono prodotti a livello commerciale. Questo tipo di moduli è detto di “seconda generazione” e ha efficienza inferiore al silicio cristallino, ma rappresenta un significativo progresso per i prodotti a film sottile.

Silicio monocristallino

Il silicio utilizzato per produrre celle fotovoltaiche ha tipicamente una purezza del 99.99999%, simile a quello utilizzato nell'industria elettronica per produrre componenti a semiconduttore (diodi, transistor, chip). Il singolo cristallo viene prodotto attraverso il metodo *Czochralski* (*CZ*), molto semplice da visualizzare. Grossi pezzi di silicio puro senza una particolare struttura cristallina vengono fusi a temperature superiori a 1414°C in un crogiolo di grafite. Un piccolo seme di silicio viene portato a contatto con la superficie del fuso per iniziare la cristallizzazione. Il silicio fuso solidifica all'interfaccia tra il seme ed il fuso mentre il seme viene lentamente ritirato. Un grosso lingotto inizia a crescere verticalmente e lateralmente con gli atomi che tendono a disporsi in un reticolo cristallino perfetto. Sfortunatamente questo metodo presenta alcuni svantaggi. La crescita del cristallo è molto lenta e comporta un elevato consumo di energia, portando ad un elevato costo di produzione. Le impurità possono essere presenti a causa dell'interazione tra il fuso ed il crogiolo. Inoltre la produzione di wafer sottili comporta il taglio del lingotto in fette, un processo molto lungo

e con lo scarto di molto materiale che può essere invece utilizzato. Per queste ragioni l'industria fotovoltaica ha incentivato la ricerca di metodi alternativi come, ad esempio, la produzione di cristalli in fogli sottili. Alcuni di questi metodi sono oggi utilizzati per produzioni a livello industriale.



Figura 1. Silicio puro prima della fusione.

Silicio policristallino

Come è stato detto in precedenza, le celle solari in silicio policristallino nascono anch'esse dal silicio puro fuso che viene però solidificato in blocchi, tagliato in mattoncini più piccoli ed infine ridotto in sottili wafer. Il processo di fusione e solidificazione produce una struttura policristallina che si allontana dalla struttura monocristallina ideale ma che viene compensata da un costo inferiore. Inoltre, dato che le celle vengono tagliate in forma quadrata o rettangolare, possono essere disposte l'una vicino all'altra nei moduli. Quando il silicio fuso si raffredda, la cristallizzazione avviene simultaneamente in diversi punti del fuso producendo grani con dimensione, forma ed orientazione casuali. All'interno di ogni grano la struttura cristallina è molto regolare, ma i bordi grano rappresentano delle imperfezioni che favoriscono la ricombinazione tra elettroni e lacune.

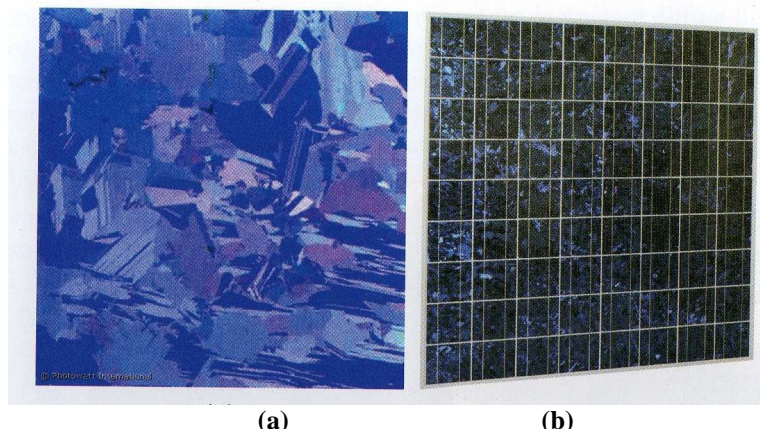


Figura 2. Wafer di silicio policristallino (a) e modulo fotovoltaico in silicio policristallino (b)

Vincoli progettuali

I progettisti di celle solari sono sempre concentrati al miglioramento dell'efficienza di conversione delle celle in silicio cristallino, cercando anche di superare gli schemi base già conosciuti. Molti dei vincoli all'efficienza sono causati dai principi di ottica e di teoria quantica, altri dalle proprietà dei materiali semiconduttori o dai problemi di progetto. La figura ... sintetizza i principali fattori che determinano l'efficienza di una tipica cella solare in silicio in commercio che opera alla massima potenza. La potenza solare incidente è denotata con 100% e le successive perdite riducono la potenza disponibile attorno al 15-20% in uscita.

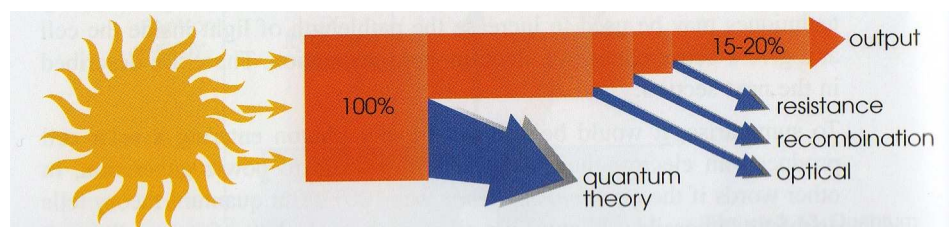


Figura 3. Perdite di efficienza di una cella fotovoltaica.

Teoria quantica

Questo argomento rappresenta la più grande perdita di efficienza delle celle basate su una singola giunzione p-n. Un modo per ridurre il problema è quello di impilare due o più giunzioni con diversi gap di banda per creare una cella *tandem*.

Ottica

Le perdite ottiche riguardano la luce incidente, impedendone l'assorbimento da parte del semiconduttore e la conseguente produzione di coppie elettrone-lacuna. In una cella ci sono

tre principali tipi di perdite ottiche. Il primo tipo può essere considerato quello riguardante il bloccaggio della luce incidente da parte dei contatti superiori. L'ombreggiamento dovuto alla presenza dei contatti può ovviamente essere ridotto riducendo l'area totale occupata da questi contatti. Chiaramente, una griglia di contatti ben spaziata riduce le perdite ottiche ma ha come svantaggio quello di incrementare la resistenza. La perdita per ombreggiamento dovuto ai contatti si aggira tra l'8 e il 12%. Il secondo tipo di perdita ottica è quella associata alla riflessione della superficie superiore della cella. Per compensare questo tipo di perdita ci sono due miglioramenti progettuali applicabili. Il primo è quello di applicare un rivestimento antiriflesso, trasparente e dielettrico sulla superficie: se il rivestimento è spesso un quarto della lunghezza d'onda incidente, la luce riflessa dall'interfaccia tra il rivestimento e la cella è sfasata di 180° rispetto a quella riflessa dalla superficie superiore. L'interferenza risultante ha come effetto la cancellazione. Ovviamente, l'esatta cancellazione si verifica solamente per un valore di lunghezza d'onda, normalmente scelto pari al picco di flusso dei fotoni: $0.65 \mu\text{m}$. Il secondo miglioramento progettuale applicabile è quello di creare una *texture* sulla superficie che permetta una riflessione casuale con una maggiore possibilità da parte della luce di entrare all'interno della cella. La struttura cristallina del silicio permette, con attenti attacchi chimici, di creare delle piccole sporgenze piramidali: la luce riflessa dalle facce inclinate può incidere le piramidi vicine ed entrare nella cella. Il terzo tipo di perdita ottica è data dalla riflessione della faccia inferiore della cella senza il successivo assorbimento. Il rimedio più utilizzato è quello di applicare una superficie irregolare totalmente riflettente che possa deviare la luce in maniera casuale all'interno della cella. La luce verrà poi intrappolata per totale riflessione interna. Questo processo è detto *light trapping*.

Ricombinazione

Questo processo avviene quando gli elettroni e le lacune generati dalla luce, invece che passare attraverso la giunzione ed essere catturati dai contatti, si incontrano e si annullano. La perdita di portatori di carica influisce negativamente sia sul voltaggi che sulla corrente in uscita dalla cella, riducendone l'efficienza. Alcuni tipi di ricombinazione hanno luogo nel corpo della cella (bulk recombination) ma la maggior parte si ha in corrispondenza di impurità e difetti presenti nella struttura cristallina.

Resistenza

L'ultimo tipo di perdita è dato dalla resistenza elettrica. Una cella solare può essere considerata come un generatore di corrente. Come per tutti i generatori di corrente, è desiderabile minimizzare il più possibile la resistenza in serie ai terminali di uscita. In questo caso, l'interpretazione fisica della resistenza in serie è data da tutti i contatti e i conduttori che permettono di raccogliere il flusso di corrente in uscita, nonché dal materiale semiconduttore della cella.

Le tecniche per contrastare le perdite di efficienza nel silicio cristallino sono state raggiunte e migliorate con anni di ricerca e sviluppo in tutti i laboratori del mondo, ma il grado in cui esse vengono impiegate a livello industriale e commerciale dipende dal giudizio dei produttori: il numero e la complessità delle operazioni di processo hanno un grande impatto sui costi ed è sempre presente un inevitabile compromesso tra costi e prestazioni.

Dislocazioni nel silicio policristallino

Le dislocazioni sono responsabili del comportamento plastico dei materiali cristallini ma ne possono influenzare significativamente anche le proprietà elettriche, specialmente nel caso dei semiconduttori. Ci sono due tipi principali di dislocazioni: *edge* e *screw*. Il vettore di Burgers rappresenta l'intensità e la direzione della distorsione del reticolo cristallino causata dalla dislocazione. In una dislocazione *edge* il vettore di Burgers è normale alla linea di dislocazione mentre in una dislocazione *screw* è parallelo alla linea di dislocazione (vedi Figura 4). Tuttavia, la maggior parte delle dislocazioni è di tipo misto. Le impurità sono attratte dalle dislocazioni e agglomerati di impurità spesso creano precipitati che possono bloccare l'ulteriore moto delle dislocazioni.

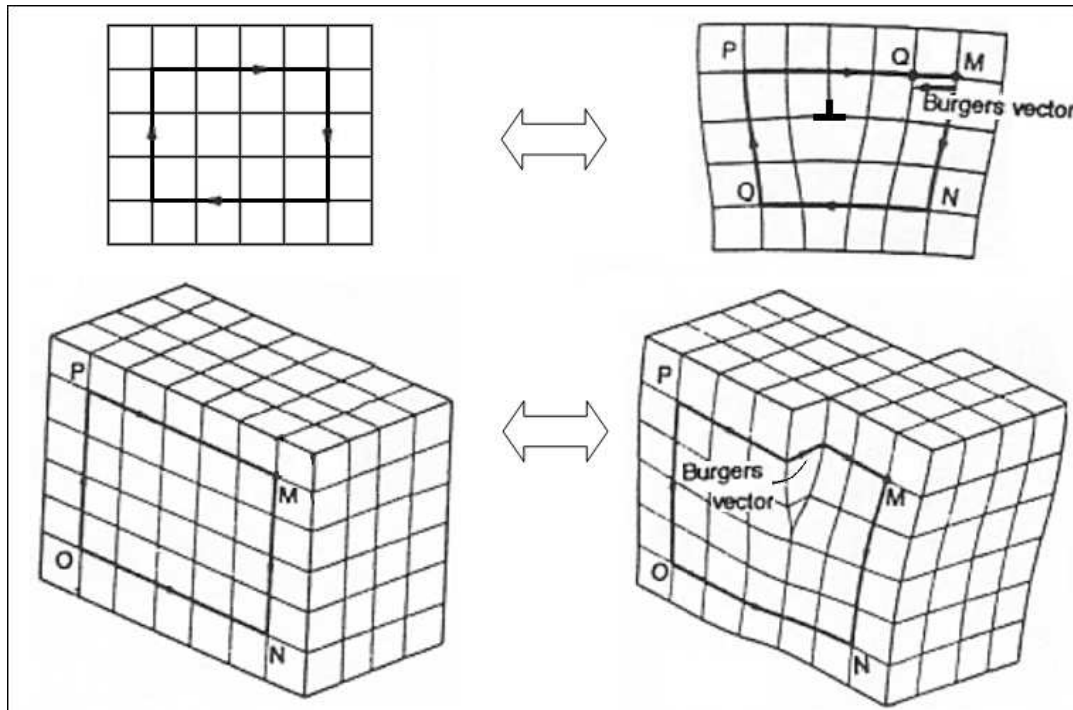


Figura 4. Direzione del vettore di Burgers in una dislocazione *edge* (in alto a destra) e in una dislocazione *screw* (in basso a destra).

Nucleazione delle dislocazioni

Ci sono diversi meccanismi di nucleazione delle dislocazioni durante la crescita e il raffreddamento della struttura cristallina. È noto che le dislocazioni possono generare come risultato della tensione prodotta attorno all'inclusione a causa della differenza tra la contrazione termica del cristallo e quella dell'inclusione stessa. Le dislocazioni possono generare anche dai bordi grano: durante la crescita ed il successivo raffreddamento si generano campi di tensione quando grani aventi differente orientazione crescono l'uno affianco all'altro, specialmente quando tre o più grani si incontrano. Anche i bordi grano in movimento possono generare dislocazioni: quando un grano cresce a spese di un altro l'impacchettamento degli atomi al bordo grano permette la nucleazione delle dislocazioni.

Movimento delle dislocazioni

Nei semiconduttori la velocità delle dislocazioni aumenta con la temperatura a parità di tensione applicata. Esistono due tipi principali di moto delle dislocazioni: *glide* e *climb*. Il *glide*, o moto conservativo, si ha quando la dislocazione si muove sul piano che contiene sia la linea di dislocazione che il vettore di Burgers. Questo processo implica lo spostamento di un piano atomico sull'altro ma il numero di atomi e di spazi nel reticolo cristallino resta invariato, per questo è detto anche processo conservativo. Il *climb*, o moto non-conservativo,

è il movimento della dislocazione fuori dalla superficie di scorrimento in direzione normale al vettore di Burgers. Il *climb* necessita di un processo di diffusione o della presenza di siti vacanti nel reticolo cristallino. Alle basse temperature la diffusione è ridotta e il moto delle dislocazioni è limitato solo al processo di *glide*. È stato studiato che un aumento della velocità delle dislocazioni è determinato solamente dagli elementi cosiddetti donatori, come il fosforo, mentre non è influenzata dagli elementi “accettatori” come il boro. Se l’impurità presente nel silicio è rappresentata da un singolo atomo, l’energia necessaria alla dislocazione per superarla non è così elevata da influire sul moto della dislocazione stessa. È quindi pensabile che gli ostacoli che rallentano e bloccano il moto delle dislocazioni siano agglomerati di impurità.

Dislocazioni contaminate da impurità

I portatori di carica che si generano in una cella solare ne determinano la corrente in uscita. Di conseguenza, una barriera alla formazione o una perdita di queste cariche diminuisce l’efficienza della cella solare. Le impurità metalliche sono comuni nel silicio cristallino di grado fotovoltaico e studi effettuati su lingotti sottoposti a solidificazione direzionale hanno rivelato la presenza di impurità quali ferro, cromo, rame, molibdeno e cobalto. Le dislocazioni possono essere spesso sito di attrazione per questo tipo di impurità ed è stato dimostrato che sono molto più dannose nei confronti dei portatori di cariche che le dislocazioni “pulite”. I precipitati metallici risultano essere dannosi in quanto aumentano la ricombinazione dei portatori di carica e diminuiscono l’efficienza della cella fotovoltaica.

Descrizione dello studio effettuato

Meccanismi di rafforzamento del silicio policristallino

Il presente lavoro si propone di studiare l'effetto che hanno due tipi di rafforzamento solitamente utilizzati in metallurgia sulle caratteristiche elettriche e microstrutturali del silicio policristallino. Tutti i meccanismi di rafforzamento introducono dislocazioni o difetti nel reticolo cristallino che agiscono da barriere allo scorrimento tra i piani atomici. I due meccanismi considerati sono il rafforzamento per soluzione solida (alligazione) e il rafforzamento per precipitazione.

Rafforzamento per soluzione solida

Questa tecnica consiste nell'aggiungere atomi di un elemento (elemento alligante) nel reticolo cristallino di un altro elemento (metallo base). L'elemento alligante diffonde nella matrice formando una soluzione solida e producendo campi di tensione locale che interagiscono con gli omologhi campi di forza generati dalle dislocazioni. In questo modo il moto delle dislocazioni viene ostacolato e la tensione di snervamento del materiale aumenta. La soluzione solida può essere di tipo sostitutivo o interstiziale ma, in entrambi i casi, l'intera struttura cristallina rimane pressoché invariata. Nella soluzione solida di tipo sostitutivo gli atomi di soluto hanno dimensioni tali da poter sostituire gli atomi del metallo base nel reticolo cristallino. Secondo le regole di Hume-Rothery, il raggio atomico dei due elementi non deve differire di più del 15% affinché abbia luogo questo tipo di soluzione. I campi generati sono di compressione e sferici e non interagiscono con le dislocazioni a vite perché privi di componente di taglio (caratteristica di questo tipo di dislocazioni). Nel rafforzamento di tipo interstiziale l'atomo di soluto ha dimensioni inferiori alla metà dell'atomo del metallo base e si annida negli spazi all'interno del reticolo cristallino causando un campo di tensione. Questo tipo di campo genera una distorsione tetragonale che può interagire con qualsiasi tipo di dislocazione. Il rafforzamento per soluzione solida aumenta la tensione di snervamento del materiale in quanto aumenta la forza necessaria al moto delle dislocazioni. Il rafforzamento del silicio per soluzione solida è possibile con elementi elettricamente inerti e completamente solubili nel silicio. Il germanio è un elemento elettricamente inerte nei confronti del silicio e il diagramma di fase Ge-Si (Figura 5) evidenzia anche la completa solubilità tra i due materiali, quindi il germanio è un elemento adatto al rafforzamento per soluzione solida del silicio. Le dislocazioni che vengono bloccate dai campi di tensione generati dagli atomi di

germanio possono prevenire l'ulteriore propagazione o moltiplicazione di altre dislocazioni. Inoltre, nel caso di silicio drogato con elevate quantità di boro, gli atomi di germanio compensano il ritiro del reticolo cristallino dovuto alla dimensione ridotta degli atomi di boro.

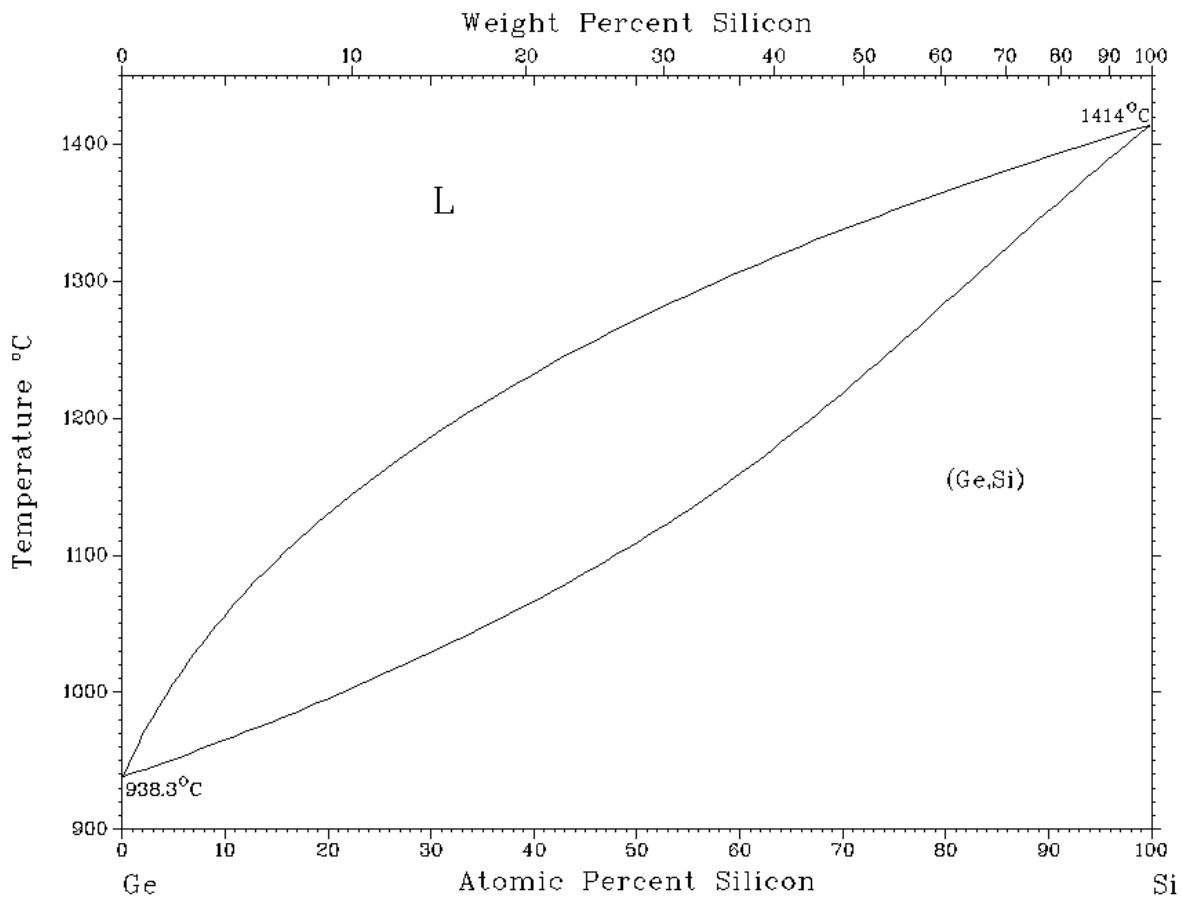


Figura 5. Diagramma di fase Ge-Si.

Rafforzamento per precipitazione

Questo metodo si basa sul cambiamento di solubilità allo stato solido in base alla temperatura. Quando la solubilità di un elemento in lega cambia, si ha la precipitazione di una fase secondaria che impedisce il moto delle dislocazioni all'interno del reticolo cristallino. Quando i precipitati differiscono in dimensione rispetto agli atomi del metallo base si ha una distorsione del reticolo: i precipitati più piccoli portano ad una tensione positiva mentre i precipitati più grandi ad una tensione di compressione. La forza che agisce sulle dislocazioni è sempre perpendicolare alla linea di dislocazione e quest'ultima, se la tensione di taglio sul piano di scorrimento è piccola, assume una forma “a bolla”. Se la tensione di taglio raggiunge il limite critico, le bolle confinanti si toccano e reagiscono a formare un anello di dislocazione attorno al precipitato e una nuova linea di dislocazione. Questo comportamento è illustrato in

Figura 6. In generale qualsiasi materiale può essere rinforzato per precipitazione ma se i precipitati sono troppo piccoli le dislocazioni possono tagliare il precipitato senza che esso si opponga al moto.

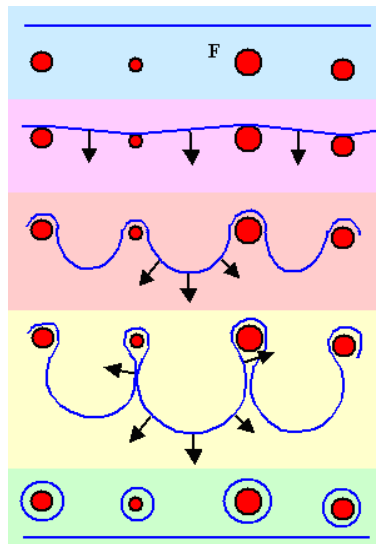


Figura 6. Rappresentazione di una linea di dislocazione che si aggancia ai precipitati.

Un altro elemento elettricamente inerte nel silicio è l'afnio e il diagramma di fase Hf-Si suggerisce che esso è anche adatto al rafforzamento per precipitazione se presente in determinate concentrazioni. Per concentrazioni di Hf fino al 30% la struttura del materiale presenta precipitati di HfSi_2 in una matrice di eutettico Hf-Si.

Preparazione dei campioni

Per verificare l'influenza del germanio sulle proprietà strutturali del silicio policristallino, sono stati studiati sette campioni drogati *p* (con aggiunta di boro) intenzionalmente legati con germanio fino all'1% in peso. Ciascun campione consiste in una fetta dello spessore di 2 mm ricavata dalle parte centrale di un lingotto di 6 cm di diametro e dell'altezza di 5 cm. Ogni lingotto è stato fuso in un forno Bridgman da laboratorio nell' Istituto di Metalli Non Ferrosi e Materiali Super Puri all'Università di Freiberg in Germania. Per verificare l'effetto del metodo di rafforzamento per precipitazione, sono stati studiati due ulteriori campioni. Questi due campioni, ottenuti nello stesso modo dei campioni precedenti, sono stati drogati con boro e legati con afnio nelle percentuali del 6% e dell'11% in peso. Oltre a tutti i campioni sopra descritti, è stato studiato nello stesso modo un campione di riferimento senza alcun elemento in lega denominato *Si-1*. Prima di effettuare ogni misurazione i campioni devono essere

lucidati e, per le misurazioni con lo scanner laser (PV Scan), sottoposti ad attacco chimico. I campioni sono dapprima fissati su un piatto circolare di alluminio con una cera solubile in acqua. Successivamente questo supporto è montato su una macchina per la lucidatura. Questa macchina ha la caratteristica di applicare una forza costante ad una determinata velocità di rotazione mentre un disco lucidante ruota alla stessa velocità in senso opposto. La procedura di lucidatura e i parametri di lavoro sono descritti al paragrafo 4.2.1.



Figura 7. Rappresentazione dell'apparecchiatura per la lucidatura dei campioni vista da sopra (a sinistra) e il supporto del campione visto di lato (a destra).

In seguito alla lucidatura, i campioni vengono sottoposti ad attacco chimico che permette la rimozione degli atomi dalla superficie. Se il numero di atomi rimossi dalla superficie è maggiore in corrispondenza delle dislocazioni allora si formeranno delle depressioni, mentre se il numero è inferiore, si formeranno dei rigonfiamenti sulla superficie stessa. Il metodo più comune per una rimozione lenta e controllata degli atomi dalla superficie è l'utilizzo di una soluzione contenente acido fluoridrico, acido nitrico e acido acetico in un determinato rapporto. La reazione che sta alla base della dissoluzione della superficie del silicio è un ossidazione del silicio seguita dalla rimozione dello strato stesso di ossido attraverso l'acido fluoridrico. Il procedimento seguito per effettuare l'attacco chimico dei campioni è descritto al paragrafo 4.2.2.

Metodi sperimentali e risultati delle misure

Le misurazioni effettuate sui campioni si articolano in cinque diverse fasi:

- Misurazione della distribuzione di ossigeno e carbonio attraverso la strumentazione FTIR (Fourier Transform Infrared Spectroscopy);
- Misurazione della distribuzione del germanio e dell'afnio all'interno dei rispettivi campioni con strumentazione EPMA (Electron Probe Micro Analyser);
- Misurazione della resistività con la sonda a quattro punti;
- Misurazione della dimensione dei grani cristallini con il metodo ad intersezione;
- Misurazione della densità di dislocazioni con lo scanner laser (PV Scan).

Distribuzione e concentrazione di ossigeno e carbonio

La FTIR è una tecnica analitica che permette di identificare le concentrazioni di specie organiche ed inorganiche nei solidi e nei film sottili. In questa tecnica si misura l'assorbimento di varie lunghezze d'onda infrarosse da parte delle specie di interesse: determinate bande di assorbimento identificano determinate specie e strutture molecolari. La radiazione infrarossa viene fatta passare attraverso il campione e l'accoppiamento tra il legame molecolare e la radiazione ha come risultato un picco di assorbimento nello spettro misurato. Per un determinato spessore del campione, l'integrale dell'area dello spettro è proporzionale alla concentrazione della specie chimica. Per diminuire gli errori di misura viene considerata la media di una serie di spettri della stessa misurazione. Nel modo più semplice uno spettrometro in grado di effettuare questo tipo di misurazioni è composto da due specchi collocati a 90° l'uno rispetto all'altro e orientati perpendicolarmente. Uno dei due specchi è mobile, l'altro è fisso. Un prisma è posizionato al vertice dell'angolo retto e orientato a 45° rispetto ai due specchi. La radiazione che incide sul prisma viene divisa in due parti ciascuna delle quali si propaga verso gli specchi e viene poi riflessa dagli stessi. I due raggi riflessi vengono ricombinati e trasmessi al dispositivo rilevatore. Muovendo uno specchio è possibile creare un campione di comparazione che permette di codificare lo spettro della sorgente. La strumentazione è rappresentata in Figura 8.

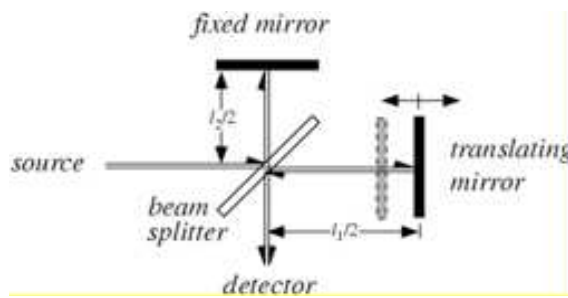


Figura 8. Rappresentazione dell'apparecchiatura FTIR.

Questa apparecchiatura permette una misura semplice e non distruttiva ed è adatta ad una stima di massima della concentrazione di ciascuna specie chimica. Le misurazioni sono state effettuate registrando lo spettro di assorbimento ogni 4 millimetri dalla parte inferiore alla parte superiore di ogni campione. Lo spettro presenta due picchi che rappresentano le concentrazioni di ossigeno e carbonio. Il picco relativo all'ossigeno è posizionato a 1107 cm^{-1} e il picco relativo al carbonio a 605 cm^{-1} . L'assorbimento è stato convertito in concentrazione (atomi/cm^3) con i coefficienti di conversione implementati nel software utilizzato. I risultati delle misurazioni sono riportati al paragrafo 5.2. Lo scopo di queste misurazioni è stato quello di verificare se i fattori normalmente coinvolti in un processo di fusione, come la concentrazione di ossigeno e carbonio, possano cambiare il loro comportamento nei lingotti contenenti germanio e afnio. Nei campioni contenenti germanio è stato possibile notare che il contenuto di ossigeno tende a diminuire spostandosi dalla parte inferiore alla parte superiore del lingotto: infatti, il coefficiente di partizione dell'ossigeno nel silicio è 1.4 e questo comportamento è quello che ci si può aspettare. Per quanto riguarda la distribuzione di carbonio negli stessi campioni, è stato possibile vedere che essa è pressoché costante per tutta l'altezza del lingotto ma è possibile pensare che la concentrazione aumenti esponenzialmente nella parte più alta a causa del coefficiente di partizione pari a 0.07. Nei campioni contenenti afnio l'ossigeno ha lo stesso andamento dei campioni precedenti mentre le misurazioni relative alla distribuzione di carbonio ne evidenziano un incremento nella parte centrale del lingotto seguito da una brusca diminuzione nella parte superiore: è possibile affermare che questo comportamento sia dovuto per lo più all'elevata presenza di precipitati che influiscono negativamente sulla misura. In definitiva si può comunque dire che la distribuzione di ossigeno e carbonio non viene influenzata dalla presenza di germanio e afnio in lega.

Distribuzione degli elementi in lega

L'EPMA è lo strumento utilizzato per analizzare la composizione chimica di un campione lucidato meccanicamente. Quando elettroni con elevata energia bombardano il campione, vengono rilasciati elettroni secondari dalle orbite più interne degli atomi che lo compongono. Gli elettroni delle orbite ad energia più elevata vanno ad occupare i posti lasciati vuoti ed emettono energia in eccesso sotto forma di raggi X. Questa energia è direttamente proporzionale al numero atomico. La strumentazione EPMA permette di rilevare la quantità di energia rilasciata e, di conseguenza, il tipo di elemento da cui proviene. In questo lavoro la strumentazione EPMA è stata utilizzata per rilevare la distribuzione degli elementi in lega, quali germanio e afnio. L'equazione di Scheil (Equazione 3) descrive la distribuzione del soluto durante la solidificazione della lega assumendo l'equilibrio in corrispondenza del fronte di solidificazione all'interfaccia solido-liquido. Se il coefficiente di partizione (k) è inferiore a 1, la concentrazione di soluto durante la solidificazione è maggiore nella frazione liquida e ci sarà un accumulo del soluto nella parte che solidifica per ultima. Al contrario, se è maggiore di 1 il soluto si accumulerà nella parte che solidifica per prima. Le misurazioni effettuate in questo lavoro hanno permesso di verificare il valore conosciuto del coefficiente di partizione del germanio nel silicio, pari a 0.33, sostituendo questo valore all'equazione di Scheil e costruendo delle curve che permettessero un confronto con i valori misurati. Nel caso dell'afnio la documentazione relativa al coefficiente di partizione nel silicio è inesistente, ma è stato comunque possibile verificare che è inferiore a 1 ed il valore che meglio si allinea alle misure effettuate è risultato essere 0.004.

Resistività

La resistività di un semiconduttore è un fattore molto importante e la sua misura è largamente effettuata in campo industriale. Il metodo utilizzato per le misure di questo elaborato si serve di una sonda a 4 punti e lo standard ASTM F43-93 e F723-97 ha permesso la conversione tra la resistività misurata e la densità dell'elemento dopante nel campione. La sonda a 4 punti viene posizionata sulla superficie piana del campione e una corrente continua viene fatta passare attraverso i due punti più esterni della sonda. La differenza di potenziale misurata tra i due punti più interni della sonda permette così di misurare la resistività del campione. Lo schema della sonda è descritto in Figura 9.

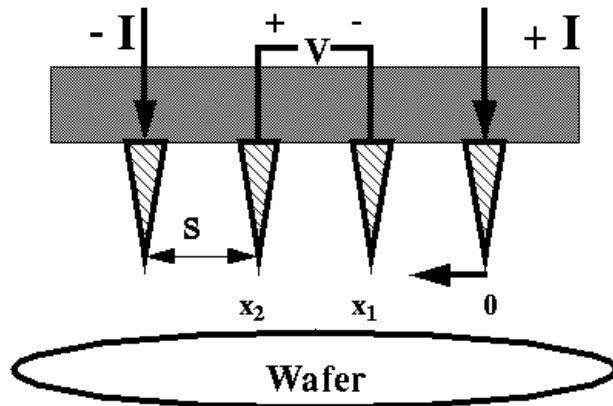


Figura 9. Sonda a quattro punti.

Le equazioni utilizzate per calcolare la resistività e la densità dell’elemento dopante sono rispettivamente l’equazione 12 e 13 (Paragrafo 4.5). Come risultato di queste misurazioni, in tutti i campioni, è stato possibile notare una diminuzione della resistività dalla parte inferiore alla parte superiore del lingotto. Questo comportamento può essere spiegato dall’accumulo di boro in corrispondenza della parte superiore del lingotto e l’equazione 13 spiega la diminuzione di resistività. È stato comunque osservato che il valore medio di resistività resta invariato a circa 10 Ωmm . Un’unica eccezione è stata rilevata nel campione con la concentrazione più elevata di afnio: il valore medio calcolato è stato di circa 2.5 Ωmm .

Dimensione del grano cristallino

La misurazione della dimensione dei grani cristallini è stata effettuata a partire da un’immagine di ogni campione ricavata con un comune scanner ottico con risoluzione minima di 600 dpi. Se il campione di silicio è stato lucidato o sottoposto ad attacco chimico, dall’immagine è possibile distinguere facilmente i bordi grano della struttura cristallina. Tuttavia, le misurazioni sono limitate perché non è possibile un’analisi quantitativa e la risoluzione raggiunge i valori che si ottengono ad occhio nudo. La dimensione del grano è un parametro molto difficile da misurare ma, nel caso di grani a crescita colonnare, il metodo più semplice è quello di tracciare sull’immagine ottenuta con lo scanner un numero di linee equidistanti perpendicolari alla direzione di crescita del grano e contare il numero di intersezioni con i bordi grano in ciascuna linea. Si ottiene così la lunghezza totale delle linee (L) e il numero totale di intersezioni (n_i) da cui è possibile ricavare un indice di dimensione del grano detto *lunghezza media di intersezione* (equazione 14). Questa definizione non considera le proprietà variabili dei bordi grano, ad esempio, nelle aree in cui sono presenti

twins, la dimensione del grano diventa molto piccola e molto difficile da misurare con questo metodo. In questo lavoro sono state tracciate linee equidistanti 5 mm sull'immagine di ogni campione e sono stati ricavati i rispettivi valori della *lunghezza media di intersezione*. Effettuando una correlazione lineare dei risultati, è stato ricavato un coefficiente di correlazione pari a 0.25. Il grafico che rappresenta i risultati ottenuti è la figura 39 (paragrafo 5.4). Questo risultato è insufficiente per affermare un collegamento diretto tra la concentrazione di germanio e la dimensione del grano cristallino di silicio. Lo stesso tipo di misura è stato effettuato per i campioni contenenti afnio ma in questo caso l'elevata presenza di precipitati nella parte superiore dei campioni ha reso impossibile la determinazione dei valori dell'indice di dimensione del grano.

Densità di dislocazioni

Il PV Scan è un'apparecchiatura che permette la misurazione della densità di dislocazioni in base alla luce riflessa dalla superficie di un campione precedentemente sottoposto ad attacco chimico. Un raggio laser illumina perpendicolarmente la superficie del campione. La luce viene riflessa dai solchi creati dall'attacco chimico e viene raccolta da una sfera che permette la misurazione. Il segnale misurato dalla sfera è direttamente proporzionale alla densità dei solchi ed è interpretato come densità di dislocazioni. La luce che colpisce un solco corrispondente ad una dislocazione viene riflessa con un angolo ampio, mentre la luce che colpisce un solco corrispondente ad un bordo grano è riflessa con un angolo stretto. I due tipi di luce riflessa vengono registrate in maniera differente e quindi i bordi grano possono essere distinti dalle dislocazioni. Nel caso di aree in cui sono presenti *twins* l'errore di misurazione può essere elevato perché vengono misurati come dislocazioni.

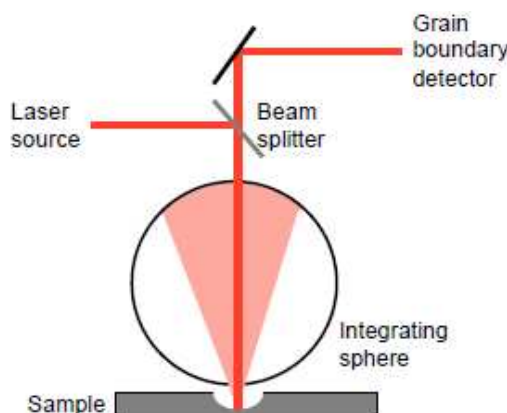


Figura 10. Riflessione con angolo ampio dovuta ad un solco di dislocazione.

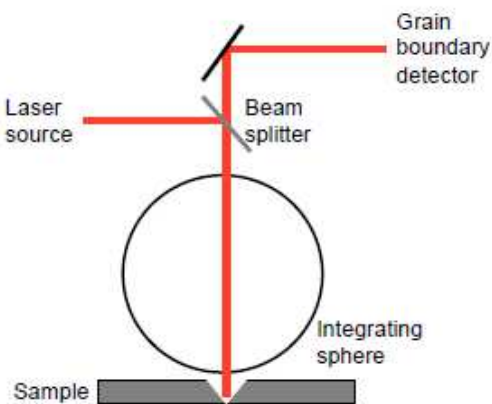


Figura 11. Riflessione con angolo stretto dovuta ad un solco di bordo grano.

Il PV Scan permette una misurazione veloce ed è l'unico metodo disponibile per ottenere misure statistiche in larga scala. I campioni devono essere lucidati e sottoposti ad attacco chimico. In questo lavoro è stata scansionata un'area di 7x7 cm con una risoluzione di 50 μm : in questo caso il software collegato all'apparecchiatura PV Scan genera una matrice di 1400x1400 valori. Ogni valore corrisponde perciò alla densità di difetti in un'area di 50x50 μm . Per eliminare la parte più esterna di ogni campione in cui si ha un accumulo di difetti, lo studio è stato ridotto ad un'area di 5x3.5 cm. I valori possono essere rappresentati su un istogramma per evidenziare la distribuzione di densità di dislocazioni e, per permettere una più facile comprensione dei risultati, è stata tracciata una curva che unisce i valori centrali di ogni intervallo dell'istogramma. I risultati sono rappresentati in Figura 12. Le misure effettuate hanno rivelato un'influenza del germanio sulla densità di dislocazioni. In particolare è stato osservato che la minima densità di dislocazioni si raggiunge nel campione con concentrazione pari allo 0.0155% in peso. Lo stesso risultato si ha osservando il valore minimo, medio e massimo della densità di dislocazioni: ognuno di questi valori raggiunge il minimo nel campione sopra citato (Figure 13, 14, 15).

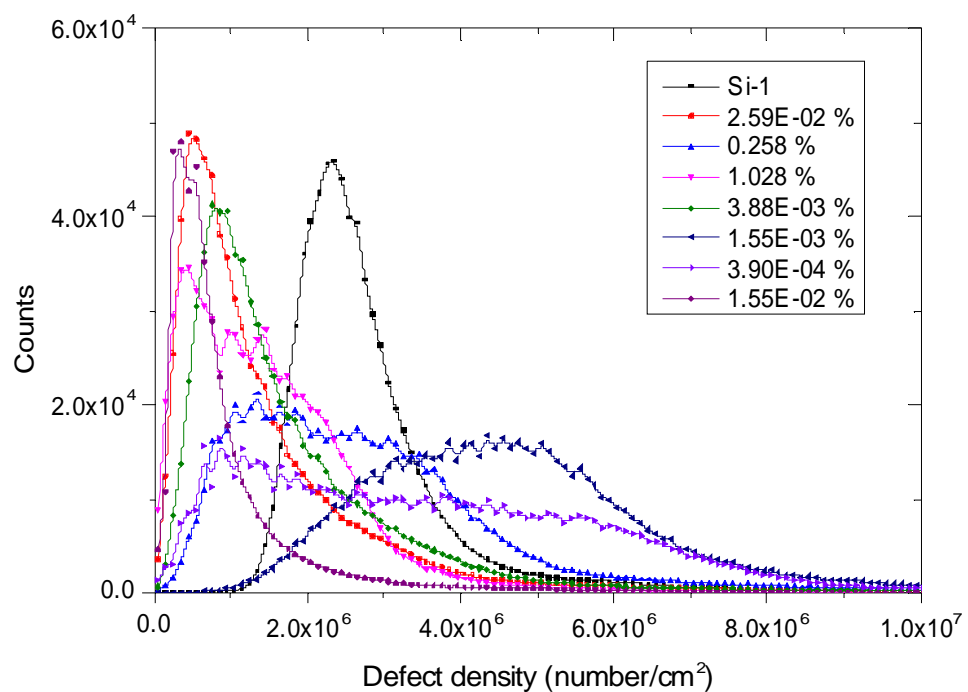


Figura 12. Distribuzione della densità di difetti nei campioni contenenti germanio.

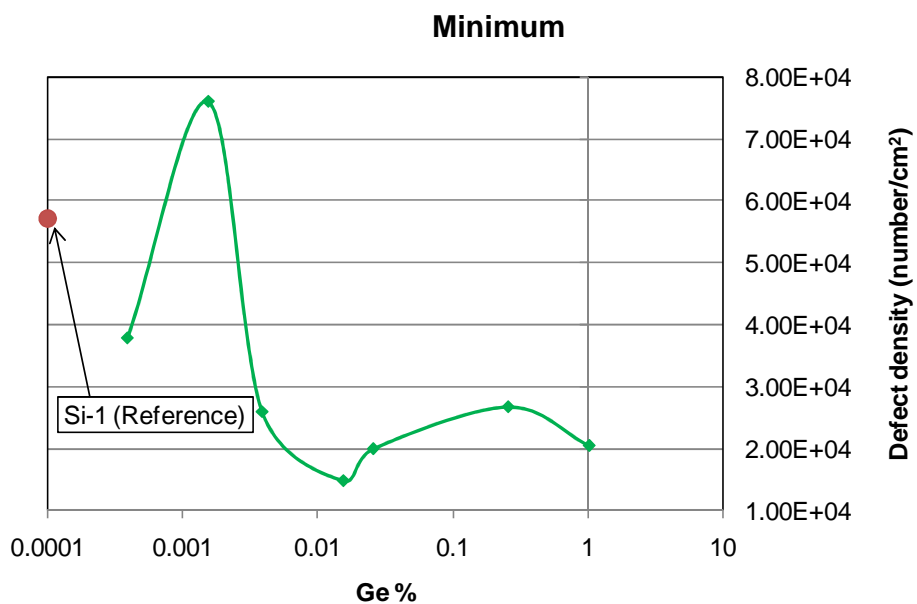


Figura 13. Valori minimi della densità di dislocazioni nei campioni contenenti germanio.

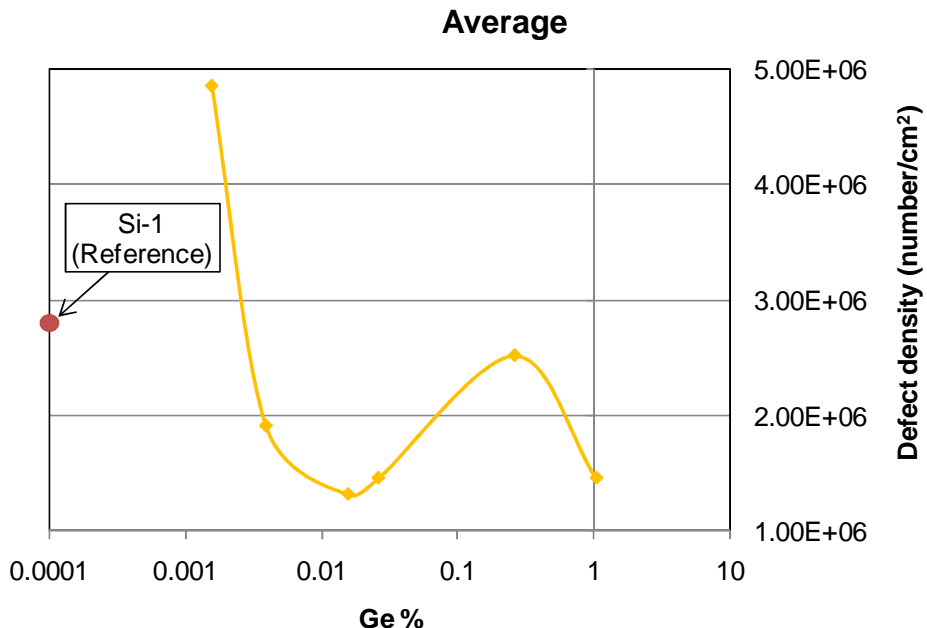


Figura 14. Valori medi della densità di dislocazioni nei campioni contenenti germanio.

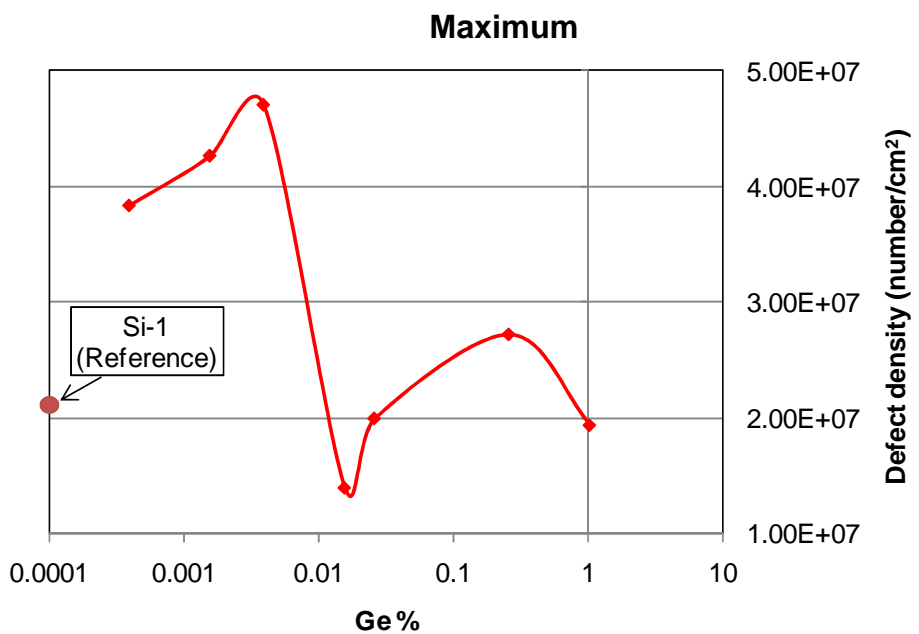


Figura 15. Valori massimi della densità di dislocazioni nei campioni contenenti germanio.

Questo risultato deve essere preso con cautela perché studi precedenti hanno dimostrato che il germanio in concentrazioni elevate riduce drasticamente le proprietà elettriche del silicio. Tuttavia, in questo lavoro la concentrazione di germanio è molto più bassa di quella considerata nei suddetti studi e perciò l'influenza sulle proprietà elettriche dovrebbe essere verificata. I risultati ottenuti sui campioni legati con afnio sono stati apparentemente confortanti ma non sono stati presi in considerazione perché l'elevata presenza di precipitati ha di certo influito e falsato le misurazioni.

Aspetti conclusivi e sviluppi futuri

Il risultato principale ottenuto da questo lavoro è stato che il germanio, in determinate concentrazioni, riduce la densità di dislocazioni nel silicio policristallino. I risultati mostrano che, oltre alla riduzione del valore medio di densità di dislocazioni, si ha una riduzione del valore minimo e massimo della stessa. L'effetto migliore si raggiunge con una concentrazione di germanio pari a 0.0155% in peso. Basse concentrazioni di germanio (inferiori all'1%) sembrano influenzare positivamente le caratteristiche strutturali del silicio policristallino ma l'influenza sulle principali proprietà elettriche non è nota. È inoltre necessario un riconoscimento delle aree in cui sono presenti *twins* per eliminarne il contributo e concentrare le misure solo sulla densità di dislocazioni. Ciò che può essere sviluppato per comprendere meglio l'effetto del germanio sulle proprietà strutturali ed elettriche del silicio, è lo studio di ulteriori campioni contenenti germanio con concentrazioni dallo 0.01% all'1% in peso. Per quanto riguarda lo studio fatto sui campioni contenenti afnio, il risultato principale è stato la diminuzione della resistività in entrambi i campioni. Nonostante l'assenza di documentazione riguardante il coefficiente di distribuzione dell'afnio nel silicio è stato possibile definire un valore che più approssima i risultati delle misure: 0.004. Le misurazioni riguardanti la dimensione del grano cristallino e la densità di dislocazioni sono state molto difficili a causa dell'elevata presenza di precipitati. Lo studio può essere approfondito diminuendo la concentrazione di afnio ed eventualmente studiando un metodo per eliminare gli errori dovuti alla presenza di precipitati dalle misure sulla densità di dislocazioni.

Table of content

Affidavit.....	3
Acknowledgement.....	5
Abstract.....	7
Extended abstract.....	9
Table of content.....	31
1 Introduction.....	33
1.1 PV research.....	33
1.2 Dislocations in Si for solar cells.....	33
1.3 Motivation of the thesis.....	33
2 Multi-crystalline Silicon.....	35
2.1 Feedstock.....	36
2.1.1 The Siemens process.....	37
2.1.2 Metallurgical refining route.....	39
2.1.3 Direct metallurgical approach.....	40
2.1.4 Purification via casting.....	41
2.1.5 Recycling.....	43
2.2 Directional solidification of mc-Si.....	45
2.3 Defect in mc-Si.....	47
2.3.1 Point defects.....	47
2.3.2 Planar defects: grain boundaries and deformation twins.....	47
2.3.3 Precipitates.....	48
2.3.4 Line defects: dislocations.....	48
2.3.4.1 Nucleation of dislocations.....	49
2.3.4.2 Dislocations mobility.....	50
2.4 Activity of dislocations contaminated by metal impurities.....	52
3 Multi-crystalline silicon strengthening mechanisms.....	53
3.1 Solid solution strengthening.....	53
3.1.1 Solid solution strengthening with Ge.....	54
3.2 Precipitation strengthening.....	55
3.2.1 Precipitation strengthening with Hf.....	56
4 Experimental methods.....	59
4.1 Sample description.....	59
4.2 Sample preparation.....	61
4.2.1 Polishing procedure.....	61
4.2.2 Etching procedure.....	62
4.3 Fourier Transform Infrared Spectroscopy (FTIR).....	62
4.4 Electron Probe Micro Analyser (EPMA).....	63
4.5 Four-point probe.....	64

4.6	Optical scanner and Intercept method.....	65
4.7	PV Scan.....	66
5	Results and discussion.....	69
5.1	Distribution of alloying elements.....	69
5.2	Oxygen and Carbon distribution.....	71
5.3	Resistivity.....	75
5.4	Grain size.....	76
5.5	Dislocation density.....	77
6	Conclusions and further works.....	81
6.1	Effect of Ge.....	81
6.2	Effect of Hf.....	81
7	References.....	83
8	Appendix A.....	87

1 Introduction

1.1 PV research

Today, thirty years later after the birth of terrestrial photovoltaic industry, crystalline silicon takes up the 91% of the whole power module market [1]. However, the current feedstock shortage does not allow a fast cost reduction as expected from the past and new technologies might get the chance to develop and to decrease the crystalline silicon domination in the PV market. Then, the solar industry is confronted to some new challenges like the presence of new impurities and the availability of new forms and shapes of feedstock.

As the raw material supply is changing, the drive for higher efficiencies and lower cost are constantly present. The E.U.'s roadmap to 2030 for silicon and PV research declares some targets for the production of multi-crystalline silicon up to 2013, such as:

- feedstock consumption up to 5 g/W_p ;
- wafer thickness less than $150 \mu\text{m}$;
- cost of $15\text{-}25 \text{ €/kg}$ dependent on quality.

To achieve these targets emphasis is given to new feedstock and defect research [2].

1.2 Dislocations in Silicon for solar cells

It is known that localised regions with high dislocation density are rather detrimental for solar cell performance. The metal impurities may easily precipitate at dislocation sites and will not be affected by standard gettering processes in the solar cell production (phosphorous diffusion and aluminium alloying), so the minority carrier lifetime will further decrease close to a dislocation. On the other hand, if dislocations are not clustered in large numbers over large areas, they may have a positive effect on the overall minority carrier acting as internal gettering sites during cooling.

1.3 Motivation of the thesis

Since the efficiency of multi-crystalline silicon (mc-Si) solar cells is mainly limited by minority carrier recombination at dislocations, if dislocation nucleation or multiplication is reduced, the efficiency will increase. It is known that metallurgical strengthening mechanisms

allow to inhibit the dislocation multiplication so, in this work, two types of these method were taken into account: solid solution strengthening by adding germanium and precipitation strengthening by adding hafnium. Investigations of Ge-doped ingots was supported by some publications already present but, in case of Hf-doped ingots, the documentation was very poor and the measurements will be useful for future works. The measurements were focused on dislocation density but also oxygen and carbon distribution, Ge and Hf distribution, resistivity and grain size were investigated. Samples from eight ingots with a different concentration of Ge and samples from two ingots with different concentration of Hf were investigated. Oxygen and carbon distribution was measured with Fourier Transform Infrared Spectroscopy (FTIR). Germanium and hafnium distribution in each sample was measured with Electron Probe Micro Analyser (EPMA). Resistivity was determined with a Four-Point probe. The grain size was determined applying a method used for ceramic materials called Intercept Method. After these measurements, samples were polished and etched in order to allow the dislocation density measurements with PV-Scan. A short summary of multi-crystalline silicon structural properties, production and defects is presented in the chapter “Multi-crystalline silicon (mc-Si)”. The theoretical basis of mc-Si strengthening mechanisms are presented in the chapter 3. All techniques concerning the samples preparation and the measuring instruments are described in the chapter “Experimental methods”. The results of the investigations are presented, discussed and summarized at the end of this thesis.

2 Multi-crystalline silicon (mc-Si)

Silicon has 4 valence electrons that allow the silicon to form bonds. Each atom can therefore bond with 4 other atoms, forming covalent bonds. Many bonded silicon atoms join together to form a single crystal of silicon. The crystal is produced from a repeating pattern from the groups of 5 silicon atoms. The arrangement of silicon atoms is repeated, forming a diamond structure and face-centred cubic (fcc) lattice. The lattice parameter, a , is 5.43 Å [4].

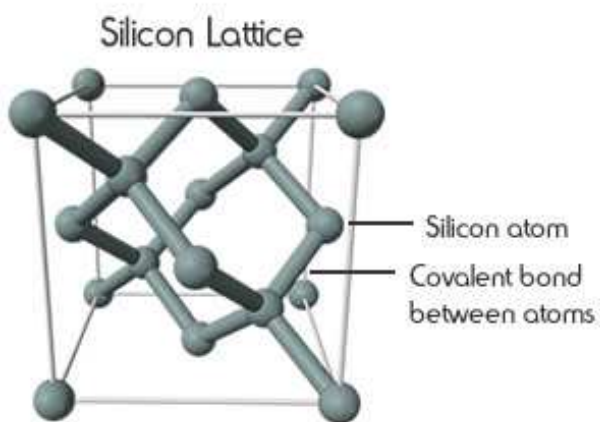


Figure 1: Schematic representation of the silicon lattice [3].

Silicon can be doped with boron or phosphorus. When silicon is doped with phosphorus, it has an extra electron that cannot fit in the outer shell of the atoms. Instead, the electron becomes detached from the atom. The additional electron can move through the lattice and therefore allow a charge to flow. Since there is an extra electron, the resulting material has a negative charge, hence it is called n-type silicon. The free phosphorus electron acts as the charge carrier.

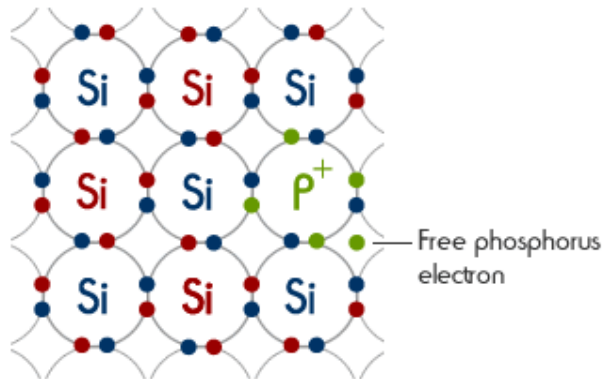


Figure 2: Phosphorous doping. Phosphorous has 5 electrons in its outer shell. When a P atom substitutes a Si atom in the lattice, 4 electrons are needed to complete the bond and a free electron is released [3].

When silicon is doped with boron, it is one electron short of completing the outer shell of the silicon and boron. This missing electron acts as a “hole”, which can move around the lattice in the same way as in intrinsic conduction. When it moves, electrons from nearby atoms can take its place, allowing current to flow. The shortage of one electron causes a positive charge in the material, therefore it is called p-type silicon.

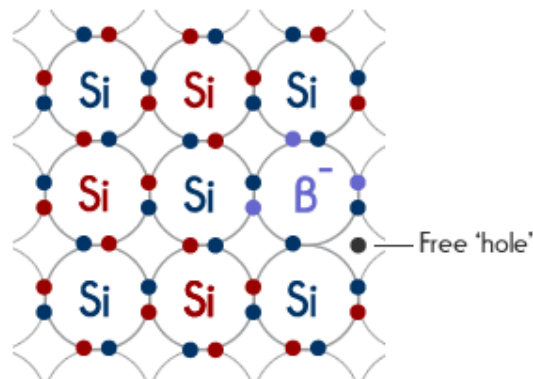
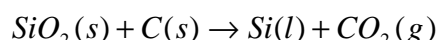


Figure 3: Boron doping. Boron has 3 electrons in its outer shell. When a B atom substitutes a Si atom in the lattice, an electron is missing and a hole is created [3].

2.1 Feedstock

Silicon is about the 28% by mass of the whole Earth's crust. However it occurs in its natural form bound to oxygen as silicon dioxide (quartz) or silicates and makes up the 75% of all rock types. Metallurgical grade (MG) silicon is produced by carbothermic reduction of quartz in an electric arc furnace [33]. The equation 1 describes the reaction.

1



The product consists of a 98-99% silicon and about 1-2% of impurities which are mainly iron, aluminium, phosphorus, calcium, titanium, carbon and boron. The consumption of electric energy is 11-13 kWh/kg produced MG-silicon. The second step in the refining of silicon provides a purity over 99% [34].

2.1.1 The Siemens process

In the Siemens process MG-Si with more than 99.6% of purity, called silgrain, is purified up to 99.9999%. Silgrain reacts with hydrogen chloride (HCl) in the presence of a copper catalyst. The main product obtained is trichlorosilane (SiHCl_3) which is purified by fractional distillation. In the presence of hydrogen, the trichlorosilane gas is decomposed and reduced at high temperature (more than 1000°C) on high-purity silicon U-shaped rods, as described by equation 2 [35].



The resulting product is polycrystalline silicon, known as electronic grade (EG) silicon, which has a typical impurity level of 10^{-9} . The Siemens process is highly energy consuming (120-160 kWh/kg produced polycrystalline silicon [36]). A sketch of the Siemens reactor is given in Figure 4.

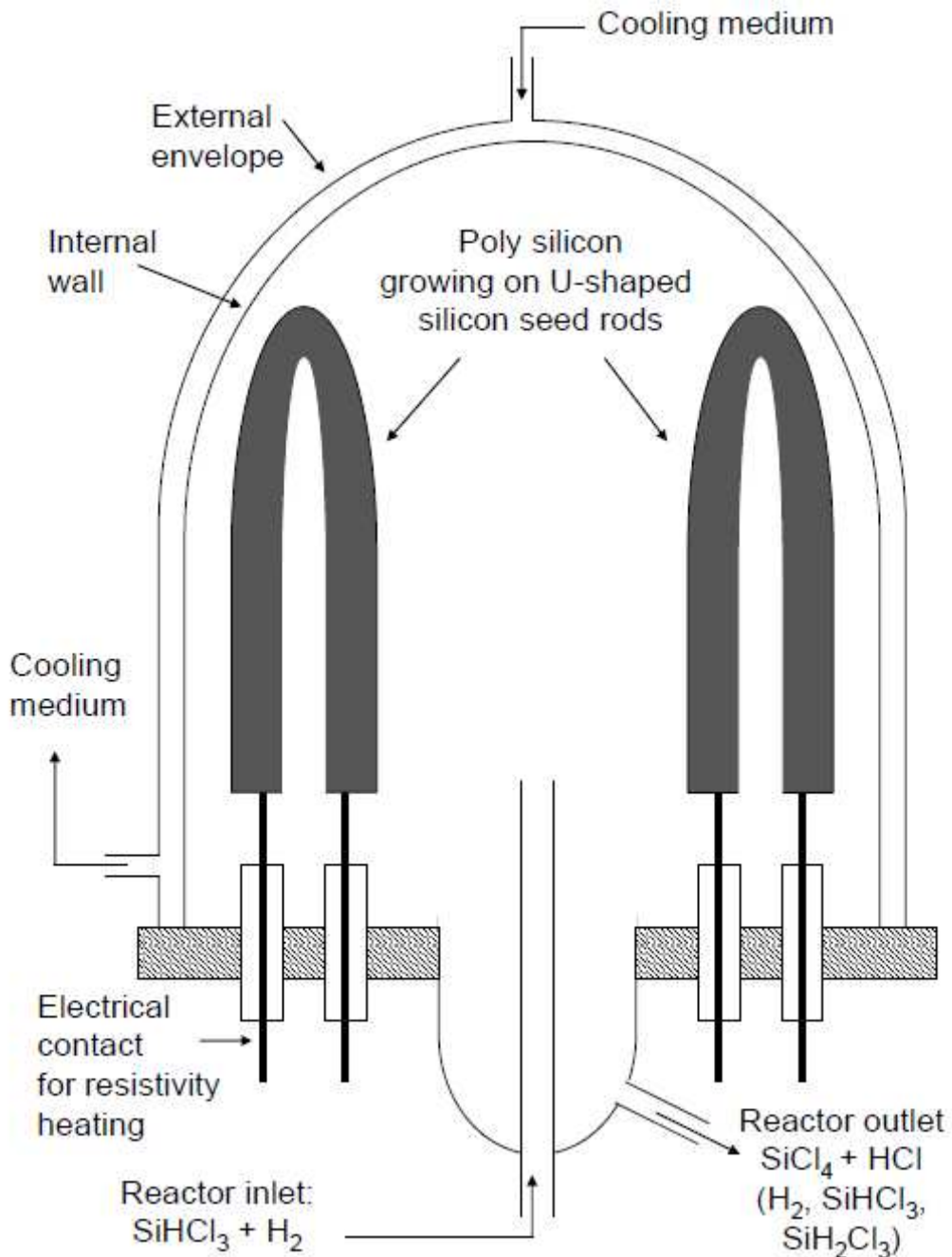


Figure 4: Sketch of a Siemens reactor used to produce polysilicon [37].

Then, from this polycrystalline silicon, ultra-pure monocrystalline silicon is obtained for the electronic industry. The top and the bottom of the silicon crystal contain small amounts of dislocations and are therefore cut off. These cut-offs and polycrystalline silicon which is not pure enough goes to the solar industry. Up to about year 2002, this was enough to cover the material need for the solar cell industry. After 2002 the demand for feedstock surpassed the supply and this has lead to a silicon shortage and a price increase as shown in Figure 5 [37].

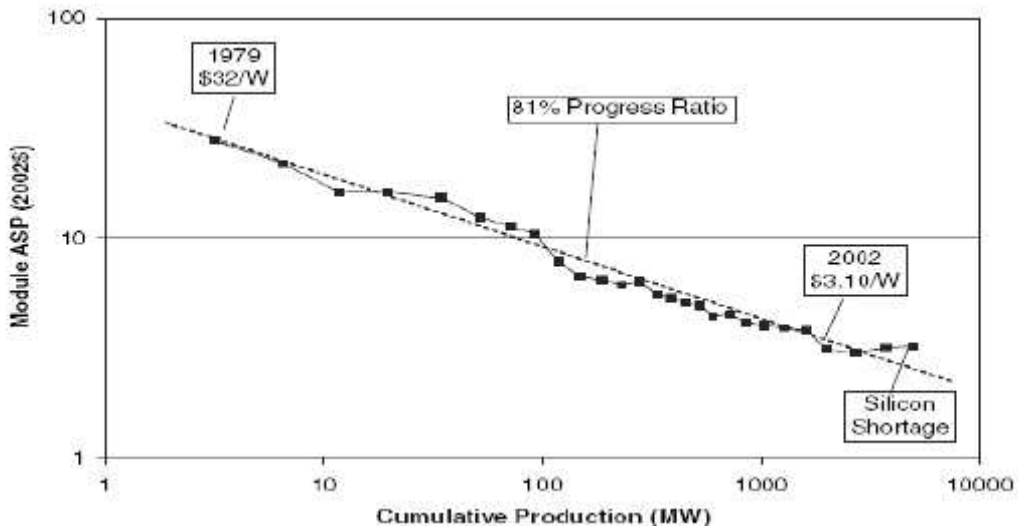


Figure 5: Historical plot of module price corrected to 2002 US dollar [38].

2.1.2 Metallurgical refining route

The metallurgical route refers to the process for silicon refining that does not involve the formation of chlorosilanes [39]. The end product of this route is called solar grade (SoG) silicon which total concentration of impurities is less than 1 ppma [40]. In spite of a higher level of impurities in the resulting silicon, the metallurgical route is assumed to be more cost effective and less energy consuming than the chemical route. The energy consumption is calculated to be 25-30 kWh/kg and the energy payback time will thus be reduced [41]. The production of SoG silicon by this route is still in the research but Elkem Solar AS has recently developed a metallurgical refining route scaled up to industrial scale. In order to produce SoG silicon, the material has to pass through three main steps: slag treatment, acid leaching and directional solidification [42]. Figure 6 shows the Elkem Solar's metallurgical refining process schematically.

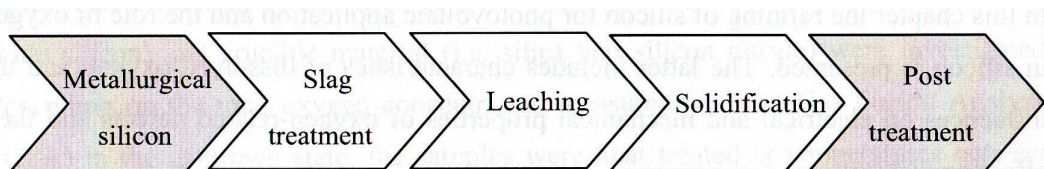


Figure 6: Elkem Solar's refining process [42].

In the first step a compound containing calcium silicide is added in a small amount to MG molten silicon. This treatment allows to extract boron from silicon. The silicon is then solidified at a relatively high cooling rate and pure crystals precipitate. The impurities remain

in the melt until the end of the solidification and segregate at grain boundaries in the alloy. The solidified silicon is crushed and purified by two leaching steps. In the first leaching step the silicon is treated with an aqueous solution of FeCl_3 or FeCl_3 and HCl which causes the disintegration of the silicon; in the second leaching step the silicon is treated with an aqueous solution of HF or HF and HNO_3 . This process will reduce impurities such as Fe, Al, Ti, P and B. Calcium is present as a potential impurity during this process but the final SoG silicon is reported to contain very little calcium [43]. In order to refine the resulting silicon, the directional solidification is used. The entire process ends with a post-treatment including cleaning and sizing of the silicon. The end product is SoG silicon classified as a compensated material because of the high amount of phosphorus (donor) and boron (acceptor) [44].

2.1.3 Direct metallurgical route

An alternative approach to the purification of MG silicon is to use high-purity raw materials in the carbothermic reduction process as ultra pure quartz and ultra pure carbon. The purity of the raw materials will greatly reduce the requirements on the purification of the silicon and thus obtain SoG silicon more directly. A process, called Solsilc, based on high purity quartz and high purity carbon black has been industrialised by Fesil Sunergy. Due to the fact that high purity raw materials come in powdered form, the process starts with a pelletizing step. The next two steps are respectively the production of SiC in a rotary plasma furnace and the production of Si from SiC in a submerged arc furnace. These two steps replace a single step in the MG silicon production where both steps are realised simultaneously in a submerged arc furnace. A schematic presentation of the Solsilc process is given in Figure 7.

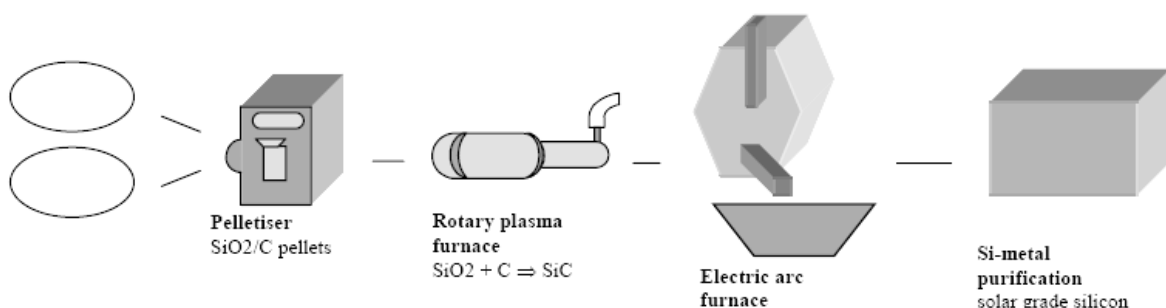


Figure 7: Process sequence of production of SoG-Si by the Solsilc process [46].

The liquid silicon which is produced by carbothermic reduction at high temperature (up to 2000°C) contains a high concentration of dissolved carbon. Virtually all of this carbon has to be removed to make the silicon suitable for ingot production. The carbon removal in the

Solsilc process begins with a controlled cooling in which the excess carbon precipitates as SiC and is separated by filtration. This results in silicon saturated with carbon at the melting point (about 70 ppmw). The carbon is then reduced to less than 5 ppmw by an oxidative melt treatment followed by solidification [47]. Figure 8 shows the approach to carbon removal in the Solsilc process. Typical yield of silicon obtained is about 70%.

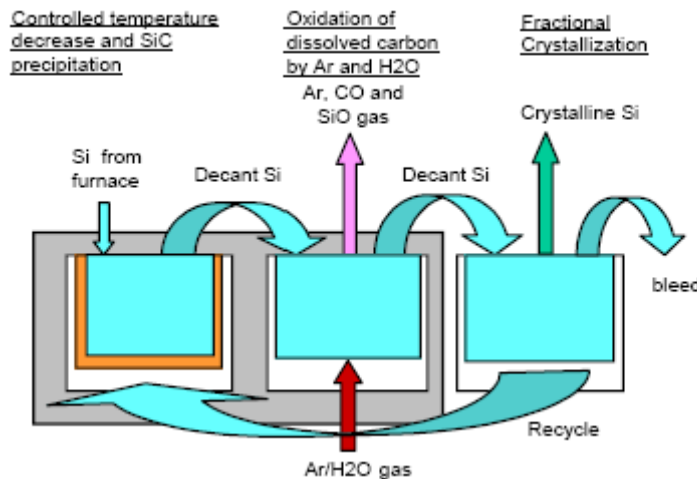


Figure 8: Carbon removal process applied after the Solsilc process [46].

2.1.4 Purification via casting

Because of the low segregation coefficient (often less than 10^{-5}) for most impurities in silicon, directional solidification is frequently used and cost-effective purifying process. Two of the impurities which are not removed by directional solidification are the common doping elements boron and phosphorus with segregation coefficient of 0.8 and 0.35 respectively [48]. Another important impurity not removed by directional solidification is oxygen that will thus largely remain in the bulk of the ingot and must be removed by other means. In directional solidification the melt reaches the solidification temperature only when the heat is dissipated at one end. The driving force of this solidification is a positive temperature gradient in the growth direction and has the opposite direction of the heat flow. Heat flow and segregation need to be controlled to maintain a good quality of the resulting mc-Si. It is necessary to control the heat flow also to obtain a planar solid-liquid interface to prevent internal stresses which, in turn, cause dislocations. When the melt solidifies from the bottom to top, since most elements are more soluble in liquid than in solid silicon, impurities dissolved in the melt will segregate and the element concentration will in most cases increase upwards in the ingot following Scheil's equation (Equation 3).

3

$$C_s = k \cdot C_0 \cdot (1 - f_s)^{k-1}$$

where

C_s : the solid composition at the solid-liquid interface;

k : equilibrium distribution coefficient;

C_0 : starting composition;

f_s : the fraction of solid.

The exponential distribution will create an heavily contaminated thin layer at the top of the resulting ingot. An example of typical distribution is shown in Figure 9.

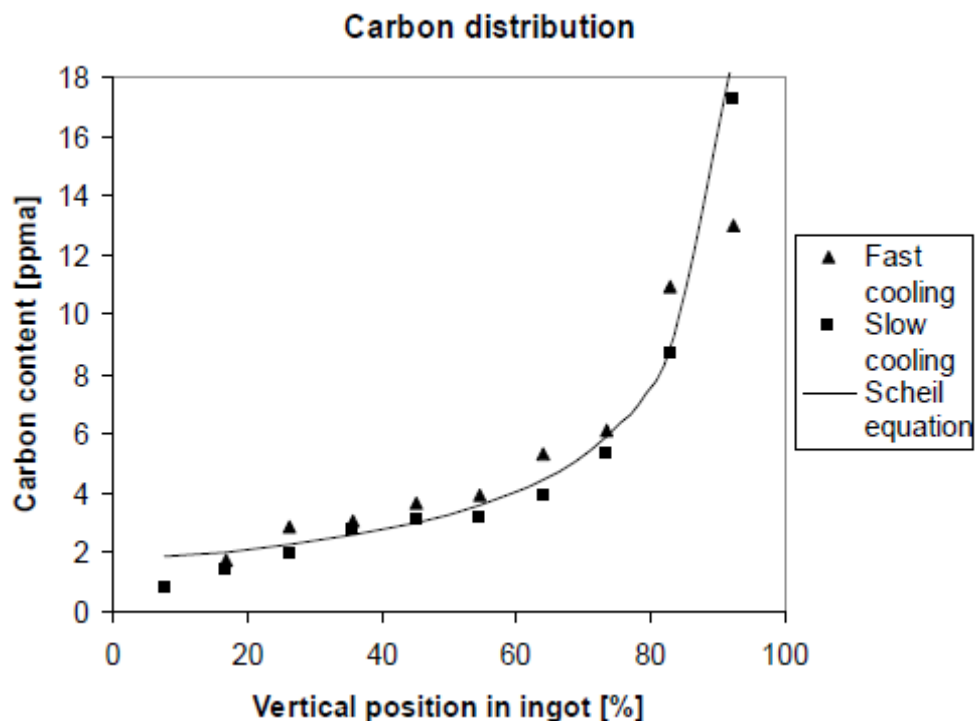


Figure 9: Carbon distribution in a directionally solidified multicrystalline ingot.

The Scheil's equation assumes no diffusion in the solid state, complete mixing in the liquid state and equilibrium at the solid-liquid interface. If convection is not sufficient, complete mixing in the liquid phase is not provided and solute atoms are rejected by the advancing solid at a greater rate than they can diffuse into the melt. Thus an enriched region, called *diffusion boundary layer*, is developed ahead of the solid. This region is denoted δ . Scheil's equation can still be used if an effective distribution coefficient, k_{eff} , is used instead of the equilibrium coefficient. The effective distribution coefficient is given by equations 4 and 5.

$$4 \quad k_{eff} = \frac{k}{k + (1-k) \cdot e^{-\Delta}}$$

$$5 \quad \Delta = \frac{v \cdot \delta}{D}$$

where

v: growth velocity;

D: diffusion coefficient of the impurity element in the liquid.

In addition to Scheil distribution, the impurity distribution will depend on diffusion. The diffusion is temperature dependent and the impurity distribution varies with varying temperature profile during growth and cooling. Impurities will diffuse into the solidified silicon from the crucible walls and bottom as well as from the coating. Back-diffusion can also occur as impurities diffuse from the heavily contaminated top layer back into the bulk material after solidification or from the boundary layer during solidification. Boron is an acceptor in silicon and mc-Si ingots made by directional solidification are often pre-doped with boron. A small amount of boron is added together with the feedstock prior to melting and solidification. Boron is most commonly used because it is the doping element with the distribution coefficient closest to 1. The distribution profile will thus not vary so much with height as the other doping elements [52].

2.1.5 Recycling

Approximately 30% of the silicon used to grow a multicrystalline ingot ends up as solar cells. Thus, it is extremely important to recycle the cut-offs, failed runs, broken wafers and kerf. After directional solidification, a carbide cut is removed from the very top of the ingot. This cut has an high impurity content due to segregation. Side, top and bottom cuts are also removed due to contamination from the crucible walls, the coating and the carbide cut layer. The carbide cut is considered waste but the side cuts together with broken wafers can be recycled by relatively simple means. Figure 10 shows the cuts removed before the wafering of the ingot.

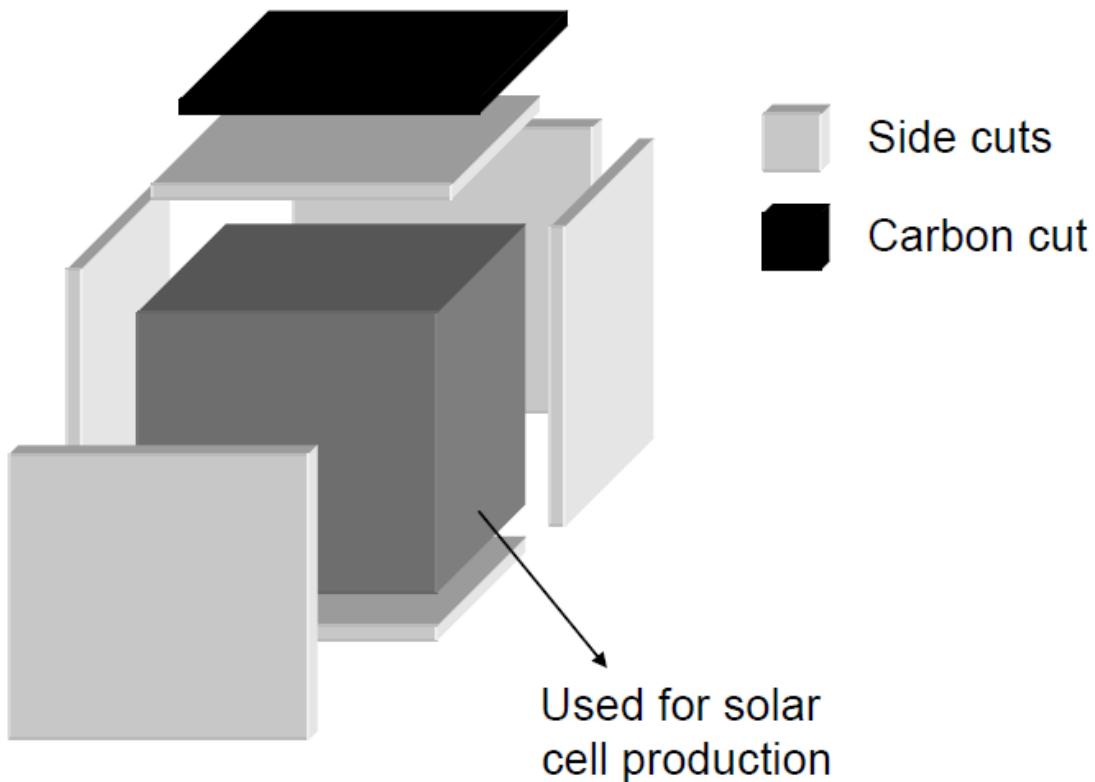


Figure 10: Sketch of the cuts removed from the ingot after solidification. Only the middle part is used for solar cell processing.

The kerf loss during wafering depends on wire thickness, carbide particle size and wafer thickness but, in the worst cases, can be as much as 50%. An European project called Recycling of Silicon rejects from PV production Cycle (RE-Si-CLE) was initiated in 1999 to demonstrate new technologies allowing for recycling of 75% of the silicon rejects in exhausted wire cutting slurries after wafering [31]. Some process steps investigated are:

- mechanical separation of SiC and liquid (polyethaneglycol or oil) from exhausted slurries by a two-step centrifugation process (SiC elimination and liquid elimination);
- magnetic removal of iron particles;
- chemical removal of iron and other metallic impurities;
- plasma purification to remove non-metallic impurities.

The amount of end-of-life photovoltaic (PV) modules is increasing and recycling of used solar cells and modules are relevant. Deutsche Solar AG in Freiberg has developed a pilot recycling plant. The recycling process consists of two main steps. First the laminate is burned off to facilitate the manual separation. In case of crystalline silicon cells, the metallisation, the antireflective coating and p-n junctions are removed subsequently by etching. After processing PV modules by thermal treatment solar cells are separated manually. Glass and

metals are supplied to their individual recycling loops. During the next step the isolated cells are chemically treated. The clean wafers, which are the final product of the recycling process, can be processed again in a standard solar cell production line and integrated into a PV module [32]. Figure 11 shows the recycling process of Deutsche Solar AG schematically.

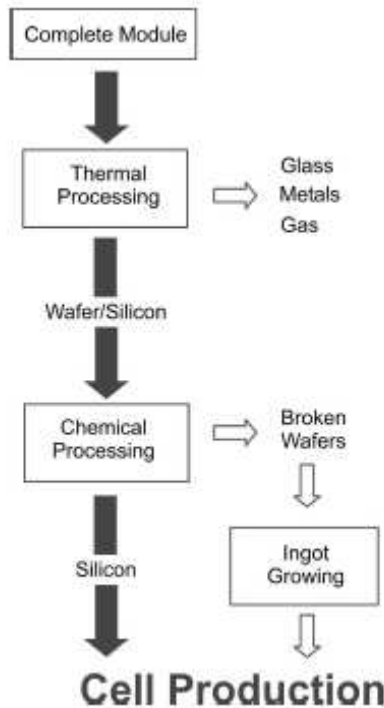


Figure 11: Principle of the recycling process of Deutsche Solar AG [32].

The energy payback time for a PV module with recycled wafers is substantially lower than the same module based on standard wafer production: 1.6 years as compared to 3.8 years if irradiation of $1000 \text{ kWh/m}^2/\text{year}$, a performance ratio of 0.75 and a module lifetime of 20 years is assumed. The environmental impact of the recycling process is argued to be lower than the other end-of-life scenarios as waste at landfill sites or shredder and sorting process [45].

2.2 Directional solidification of mc-Si

The most commonly used method for producing mc-Si is the Bridgman technique. This technique gives columnar growth and a planar solidification front. In this method the solar grade silicon (SoG-Si) feedstock is charged in a silicon nitride (Si_3N_4) coated quartz (SiO_2) crucible and heated until all the silicon is melted. Heat is then extracted from the bottom of the crucible by moving the heat zone up compared to the crucible and/or cooling the bottom

of the crucible. The solidification will start at the bottom and the solid-liquid interface moves upwards with the melt isotherm.

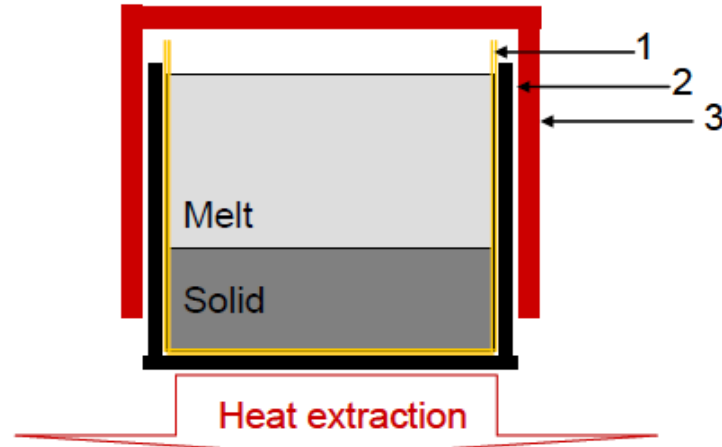


Figure 12: Sketch of directional solidification setup: 1) quartz crucible coated with silicon nitride; 2) graphite support ring and plate; 3) susceptor which is heated by induction [4].

The growth rate is proportional to the temperature gradient difference between the solid and the liquid silicon as given in equation 6 [5]:

$$6 \quad K_s \cdot G_s - K_L \cdot G_L = \rho_s \cdot H \cdot R$$

where: K_s = thermal conductivity of solid metal

K_L = thermal conductivity of liquid metal

G_s = temperature gradient in the solid at the solid-liquid interface

G_L = temperature gradient in the liquid at the solid-liquid interface

ρ_s = density of solid metal

R = growth velocity

H = heat of fusion

2.3 Defects in mc-Si

Perfect silicon crystals have periodic arrangement of atoms but in real crystals deviations from the crystal symmetry occur: these are called *defects*.

2.3.1 Point defects

These defects are localised in the vicinity of a few atoms in the crystals. A *vacancy* is a defect due to the absence of a atom on a lattice site. In a silicon crystal such a vacancy will results in four unsatisfied or dangling bonds that may recombine producing a local distortion of the lattice. Vacancies are important for nucleation of precipitates associated with an expansion in the crystal lattice. An impurity atom that replaces an atom in the host lattice is called *substitutional impurity*. The elements on group V (such as P, As, Sb, Bi) will substitute the silicon atoms in the lattice and give rise to an excess of an electron (N-doping), whereas elements from group III (such as Al, Ga or B) give rise to a deficit of bonding electrons (P-doping). Another substitutional element in silicon is carbon, but it is electrical inactive. Such atoms will sit at the interstices of the lattice and are called *interstitial atoms*. The lattice structure is relatively opened and interstitial atoms like Cu, Fe, Mn and O can easily be put inside. Interstitial atoms are often referred to as *fast diffusers* since they diffuse easily in the crystal lattice compared to substitutional atoms [6].

2.3.2 Planar defects: grain boundaries and deformation twins

Planar defects, such as grain boundaries and stacking faults, extend over an area in the material. Two grains with different crystal orientation that grow next to each other are divided by a *grain boundary*. The grains may possess some common lattice sites and the atoms occupying these sites constitute a new lattice, which is called the co-incidence site lattice (CSL). Grain boundaries with no or randomly distributed common atoms between the two grains are called non-CSL boundaries or random grain boundaries; these type of grain boundaries are more electrically active and have higher energy than the CSL-boundaries. Sub-grain boundaries in mc-Si will often exist in a much higher density than regular grain boundaries. They are constituted of a web or line of dislocations and are shown to be more electrically active than regular grain boundaries and thus more harmful for solar cell performance [7]. Twinning is a deformation mode which generates changes in the orientation of the crystal but does not affect the crystal structure. Twinning is when the crystal undergoes a change in the standing order of the [111] bonds from ...ABCABC... to ...ACBACB... . This

deformation might happen if the crystal experiences homogeneously distributed shear strain over a given region. The boundary between such a twinned area and the matrix region is called *twin boundary*. In any given crystal, twinning deformation is observed to be dominant at low temperature under high deformation rates but in silicon it is believed that most of the twins are growth twins and not deformed twins.

2.3.3 Precipitates

If impurities are present in concentrations larger than their solubility at a given temperature they may precipitate usually as compounds of silicon. Precipitates may form during solidification, during cooling after growth or during heat treatment at subsequent cell processing. Dislocation loops and stacking faults may form as a consequence of strain fields in the crystal activated by a large difference between the volume of the precipitate and the matrix volume [8].

2.3.4 Line defects: dislocations

These defects propagate as lines in the crystal. Dislocations are responsible for the plastic behaviour of the crystalline material but they may also significantly influence the electrical properties, especially in the case of semiconductors. There are two main classes of dislocations: edge dislocations and screw dislocations. The Burgers vector represents the magnitude and direction of the lattice distortion of dislocation in a crystal lattice. The vector's magnitude and direction is best understood if considering first the perfect crystal structure. In the perfect crystal structure, a rectangle whose lengths and widths are integer multiples of a (the lattice parameter) is drawn encompassing the site of the dislocation's origin. Once the dislocation is introduced in this rectangle, it will have the effect of deforming the perfect crystal structure and the rectangle as well. What was a rectangle is now an open geometric figure: the breadth of the opening defines the magnitude of the Burgers vector and, when a set of fixed coordinates is introduced, the direction of the vector may be specified. The magnitude is usually represented by equation 7:

7

$$\|b\| = \frac{a}{2} \cdot \sqrt{h^2 + k^2 + l^2}$$

Where a is the lattice parameter, $\|b\|$ is the magnitude of Burgers vector and h, k, l are the components of Burgers vector, $b = \langle h k l \rangle$ [28]. In an edge dislocation the Burgers vector is

normal to the line of dislocation whereas in a screw dislocation is parallel to the line of dislocation. Most of dislocations are, however, a mixture of the two.

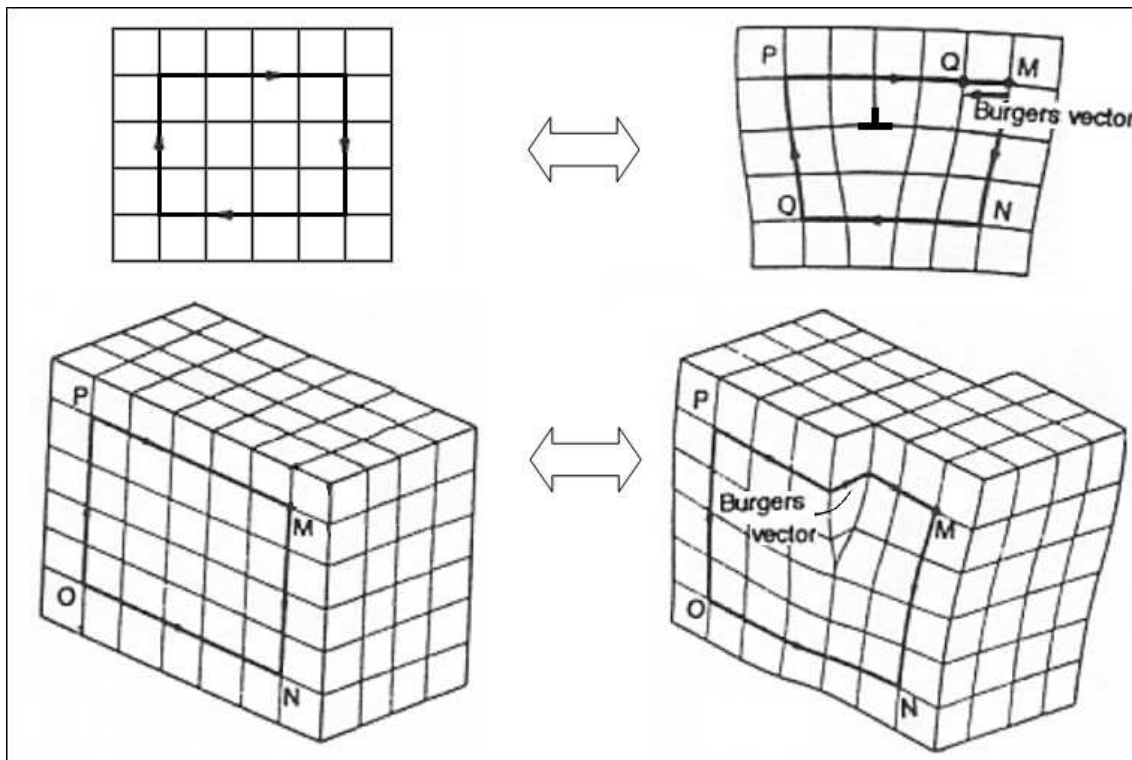


Figure 13: Direction of Burgers vector in an edge dislocation (top right) and in a screw dislocation (bottom right).

Geometrically, dangling bonds or impaired electrons are aligned along the dislocation core. Impurities are attracted to dislocations and clusters of impurities may often precipitate. Foreign atoms may influence the dislocation mobility and precipitates may pin the dislocations [9].

2.3.4.1 *Nucleation of dislocations*

There are many dislocation nucleation mechanism during the growth and the cooling of a crystal. It is known that dislocations can be generated from around an inclusion with different thermal expansion during cooling. The nucleation of dislocations results from the stress produced around the inclusion by the different contraction of the crystal and the inclusion. When the stress reaches a critical value, about $\mu/30$ (where μ is the shear modulus), dislocations are nucleated. The stress produced around an inclusion is also dependent on the inclusion size. Studies on mono-crystalline silicon showed that dislocations were generated preferentially at oxide precipitates and that the plastic flow always took place at the large

oxide precipitates for stress significantly lower than the macroscopic yield stress. As the precipitates grow in size more dislocations were produced to release the increased misfit strain associated with the precipitate. Assuming similar effect in a directional solidified multi-crystalline ingot, the precipitates might be oxides, carbides, nitrides, silicates, metallic or mixtures and the applied stress is obtained during growth and cooling after solidification. It seems that less stress is needed to punch out dislocations from bigger inclusions than from smaller ones of same kind [10]. Dislocations can also be emitted from grain boundaries and many nucleation mechanism are suggested. During growth and subsequent cooling stress fields will develop when grains with different crystallographic orientation grow next to each other and, especially, when three or more grains meet, causing what is called intra-granular and inter-granular hardening. Stress is generated by thermal expansion and contraction. A major role played by the neighbouring grains of an individual grain can be traced to the number of the surrounding grains: the more surrounding grains, the higher effect. The inter-granular effect forces the grain boundary region to deform more than the core of the grain because differences in crystallographic orientation will lead to a misfit of the slip planes in the different grains and different slip systems will be activated [11]. Dislocations generated within the grains can pile up at a grain boundary, create a large stress concentration and activate grain sources at relatively low stress applied. Also migrating grain boundaries can produce dislocations in the lattice they pass through and the dislocation density increase is dependent on the speed of movement. When one grain grows at the expense of another the packing of atoms at the grain boundary allows the nucleation of dislocations [12].

2.3.4.2 *Dislocation mobility*

In any semiconductor the dislocations velocity increases under a given stress as the temperature increases. There are two basic types of dislocation movement: glide and climb. Glide or conservative motion occurs when the dislocation moves in the plane that contains its line and the Burgers vector. Glide of many dislocations results in slip, which can be visible as steps on the crystal surface. This process involves displacement of one atom plane over another on so-called slip planes. The number of atoms and lattice sites are conserved and for this is called conservative motion. A fair number of blocks between two slip planes remains undistorted. Climb or non-conservative motion is a movement of a dislocation out of the glide surface and normal to Burgers vector. Climb requires diffusion of atoms or vacancies. At low temperatures, where diffusion is difficult, the movement of dislocations is restricted almost

entirely to climb. At high temperatures, however, an edge dislocation can move out of its slip plane by climb. The most common climb processes involve the diffusion of vacancies either towards or away from the dislocation and thus act as sources and sinks for vacancies. It has been reported that donor impurities such as P, As and Sb to enhance the mobility of dislocations [24]. The increase in dislocations velocity is determined only by the donor concentration and is not influenced by the impurity species. On the other hand, the dislocations velocity is very little modified by acceptor impurities such as B and the electrical inactive impurity, C. In impure silicon and in a low stress range, the dislocations can bow out and pass around the impurity related obstacles on the dislocation line. If the obstacle is a single atom impurity, the energy needed for a dislocation to pass around is not enough to affect the dislocation mobility, thus the obstacles that slow down dislocation motion in lower stress region are thought to be clusters or complexes of impurities. Dislocations will cease to move due to such cluster formation.

2.4 Activity of dislocations contaminated by metal impurities

Generated minority-charge carriers in a solar cell determine the amount of the output current. Therefore, a barrier to the formation or loss of these carriers decrease the efficiency of the solar cell. Metallic impurities are common in photovoltaic grade crystalline silicon and studies of directionally solidified multi-crystalline silicon revealed, for example, significant quantities of Fe, Cr, Cu, Mo and Co. Dislocations can act as gettering sites for impurities and they will very often be decorated by impurities. Decorated dislocations are often reported to be more harmful to the minority carrier lifetime than clean dislocations. Metallic contaminants are especially damaging when occurring at interstitial or substitutional lattice sites, since they may be evenly distributed throughout the wafer. Precipitated metals may also be active in terms of recombination, but at least in this case many impurity atoms are bound in one location. According to the Shockley-Read-Hall model [13], if a metal impurity produces a deep level in the band gap and has a larger capture cross section for electrons than for holes. This implies that the minority carrier lifetime should be much lower in p-type silicon than in n-type silicon. In general, metals from group 8 or less in the periodic table are donor-like and interstitial at room temperature, while those from group 9 or higher are acceptor-like and substitutional at room temperature. As a result of being donor-like the interstitial metals have large values of k (ratio of electron to hole capture cross section), while the interstitial are with $k \ll 1$. This observation has implications for their recombination strength: the interstitial metals are, generally, more detrimental in p -Si, while the substitutional metals have a greater impact in n -Si [14].

3 Multi-crystalline silicon strengthening mechanisms

As previously described, dislocations can act as gettering sites for impurities, become electrically active and decrease the efficiency of the solar cell. During the solidification process an increase of dislocation density occurs due to the mechanical stress that is present throughout the ingot. After complete cooling, the dislocation density remains constant if no external stress is applied. In metallurgy, strengthening describes techniques to increase the hardness of a material. All hardening mechanisms introduce dislocations or defects in a crystal lattice that act as barriers to slip. In this work two mechanisms to inhibit dislocation multiplication in mc-Si are considered: solid solution strengthening and precipitation strengthening [15].

3.1 Solid solution strengthening

This technique works by adding atoms of one element (alloying element) to the crystalline lattice of another element (the base metal). The alloying element diffuses into the matrix forming a solid solution and producing local stress fields that interact with those of dislocations. In this way the motion of dislocations is prevented and the yield stress of the material increases. A solid solution can be substitutional or interstitial but, in both cases, the overall crystal structure is essentially unchanged. In a substitutional strengthening the solute atom is large enough to replace solvent atoms in their lattice positions. According to Hume-Rothery rules, solvent and solute atoms must differ in atomic size by less than 15% in order to form this type of solution. In this case, generated stress fields are compressive and spherically symmetric (no shear stress component) and the solute atoms do not interact with the shear stress fields, characteristics of screw dislocations. In an interstitial strengthening the solute atom is typically less than a half the size of the solvent atom and it essentially crowds into the spaces within the lattice structure, causing defects and tensile stress fields. This kind of stress field generates a tetragonal distortion that can interact with edge, screw and mixed dislocations.

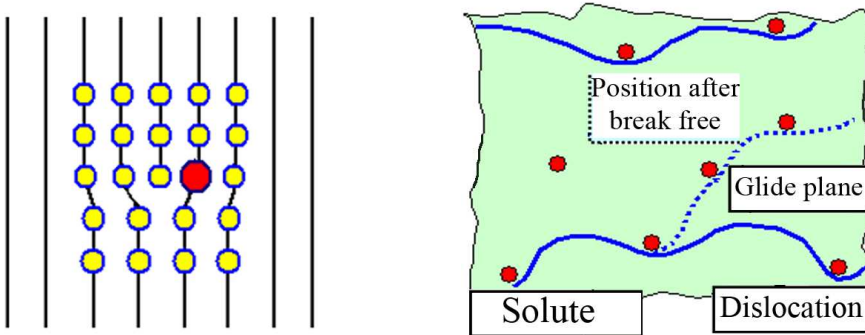


Figure 14: Effect of substitutional atoms on dislocation motion.

Solid solution strengthening increases yield strength of the material by increasing the stress to move dislocation, as given by equation 8:

$$8 \quad \Delta\tau = G \cdot b \cdot \varepsilon^{\frac{3}{2}} \cdot \sqrt{c}$$

where G is the shear modulus, b is the magnitude of Burger's vector, ε is the lattice strain due to the solute (composed of two terms: lattice distortion and local modulus change) and c is the concentration of the solute atoms. Silicon solid solution strengthening is possible with elements that are electrically inactive and with complete solubility in silicon [15].

3.1.1 Solid solution strengthening with Ge

As shown in the Ge-Si phase diagram (see Figure 15), Ge has complete solubility in silicon, thus, by adding this element to a silicon melt, the mechanism of solid solution strengthening is made. Germanium atoms are larger than silicon atoms and it is possible to argue that, as a result of temperature related stress, block or pin of dislocations may occur. Thereby, blocked dislocations may prevent further propagation or multiplication of other dislocations. Moreover, in heavily boron doped silicon, larger Ge atoms offset the crystalline shrinkage caused by boron atoms. The equilibrium distribution coefficient (k_o) of Ge in Si is 0.33 [25].

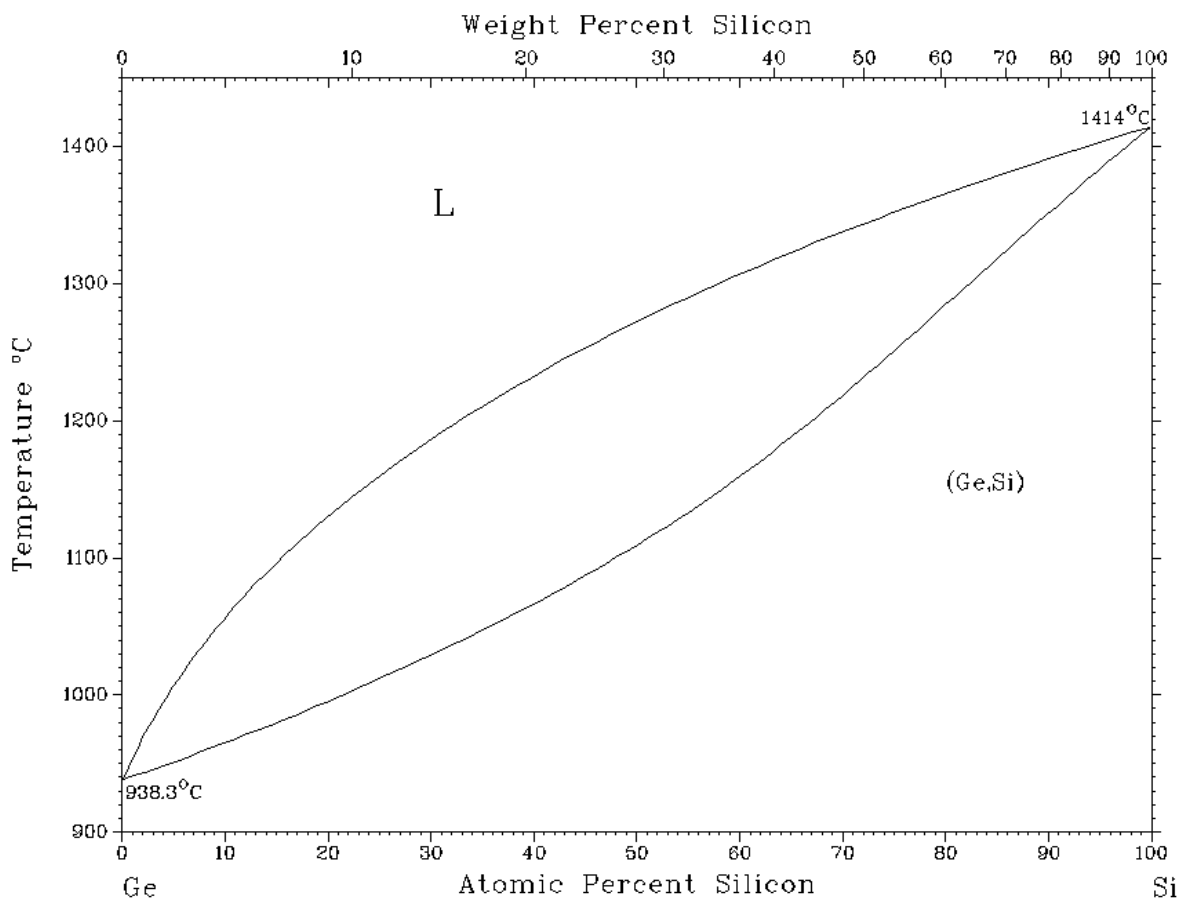


Figure 15: Ge-Si phase diagram.

3.2 *Precipitation strengthening*

This method relies on changes in solid solubility with temperature to produce fine particles of an impurity phase which impede the movement of dislocations in the lattice. Physically, this strengthening effect can be attributed both to size and modulus effects and to interfacial or surface energy. When the precipitate particles differ in size from the host atoms, there is a lattice distortion. Smaller precipitate particles in a host lattice lead to a tensile stress whereas larger precipitate particles produce a compressive stress. The dislocation pinning on the precipitates can be described by Figure 16.

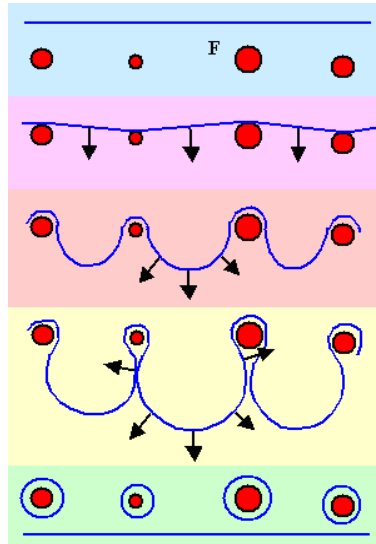


Figure 16: Representation of a dislocation line pinning precipitates.

The acting force on the dislocation is always perpendicular to the dislocation line and, if the shear stress in the glide plane is small, it takes a bulge shape. The additional stress to keep dislocations moving is given by equation 9:

$$\tau_{add} = 2 \cdot G \cdot \frac{b}{l} \quad 9$$

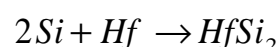
where G is the shear modulus, b the Burgers vector, l the average distance between precipitates. If the shear stress reach a critical limit, neighbouring bulges touch and react to form a dislocation loop around the precipitates and a regenerated dislocation. The main factor is the average distance between precipitates, l . Generally, every material can be hardened by many precipitations but if the precipitates are too small the dislocation may cut the precipitate. To strengthen silicon with this method, the alloying element has to be electrically inactive in silicon (four valences) and has to be able to form precipitate with the host atoms [15].

3.2.1 Precipitation strengthening with Hf

An electrical inactive element in silicon is Hafnium and the Hf-Si phase diagram in Figure 17 suggests that this element may forms precipitates if present in certain concentrations. During solidification, a concentration of Hf from 0 up to 30% allows the formation of precipitates as

the following reaction (10) explains:

10



The resulting material structure will present $HfSi_2$ precipitates in a matrix of Hf-Si eutectic.

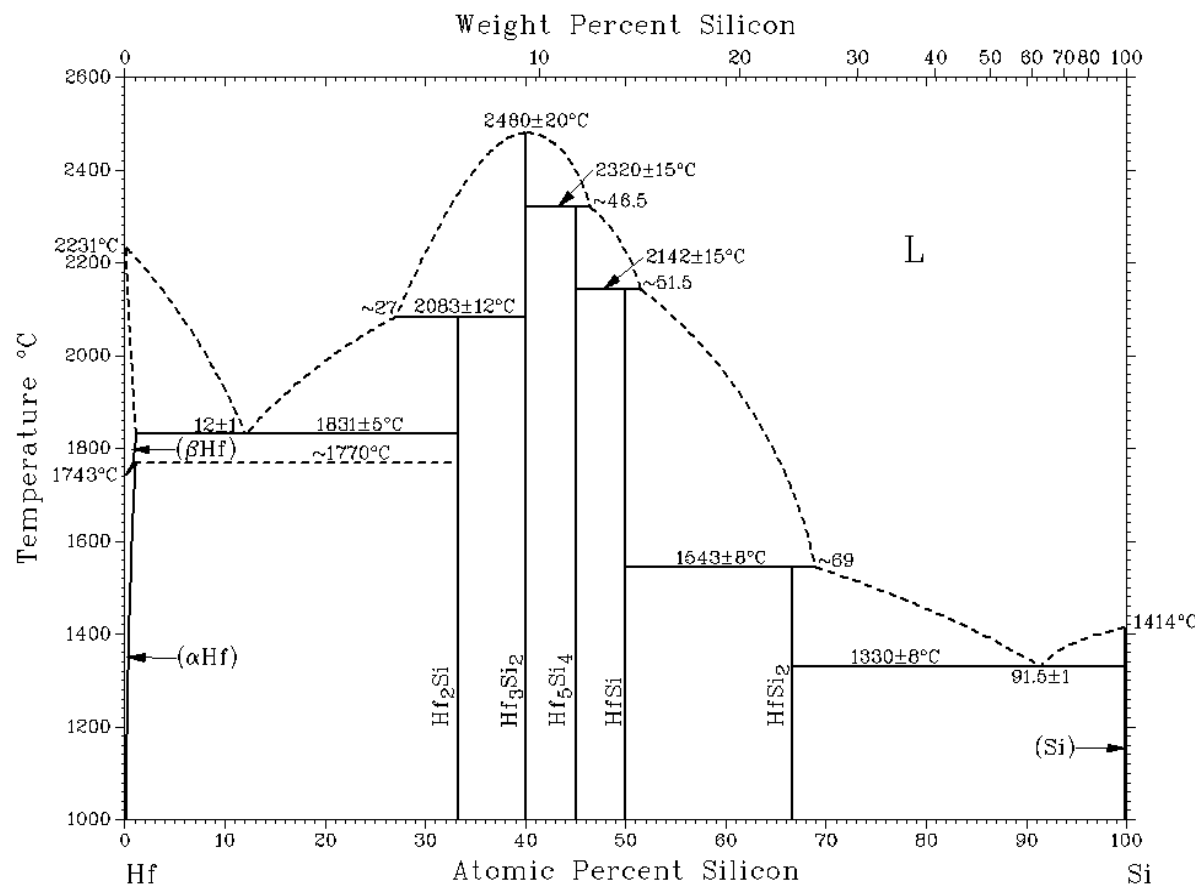


Figure 17: Hf-Si phase diagram.

4 Experimental methods

4.1 Sample description

To verify the influence of the germanium on the structural properties of multi-crystalline silicon, seven boron doped samples intentionally alloyed with germanium from 0 up to 1% of weight were studied. Each sample consist of a 2 mm thick slice cut from the central part of an ingot of 6 cm in diameter and 5 cm tall, cast in a lab-scale Bridgman furnace at the Institute of Nonferrous Metals and Super Pure Materials at TU in Freiberg. The process of casting is shown in Figure 19. The doping of the ingots has been made by adding a boron master alloy (boron content of $9.56\text{E}+19$ atoms/cm³, 0.128 ppmw) in a concentration of 0.0156% of weight (see Table 3, Appendix).

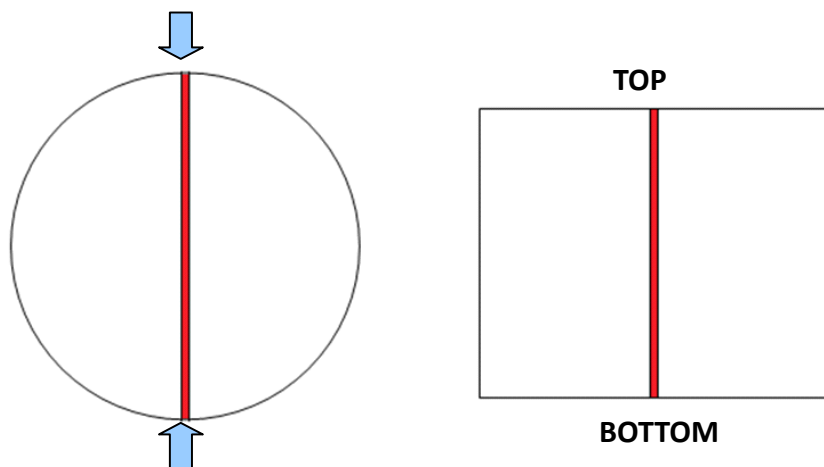


Figure 18: Sketch of the cutting of the slice with the ingot seen from the top (left) and from the side (right). The direction of cutting is parallel to the direction of solidification.

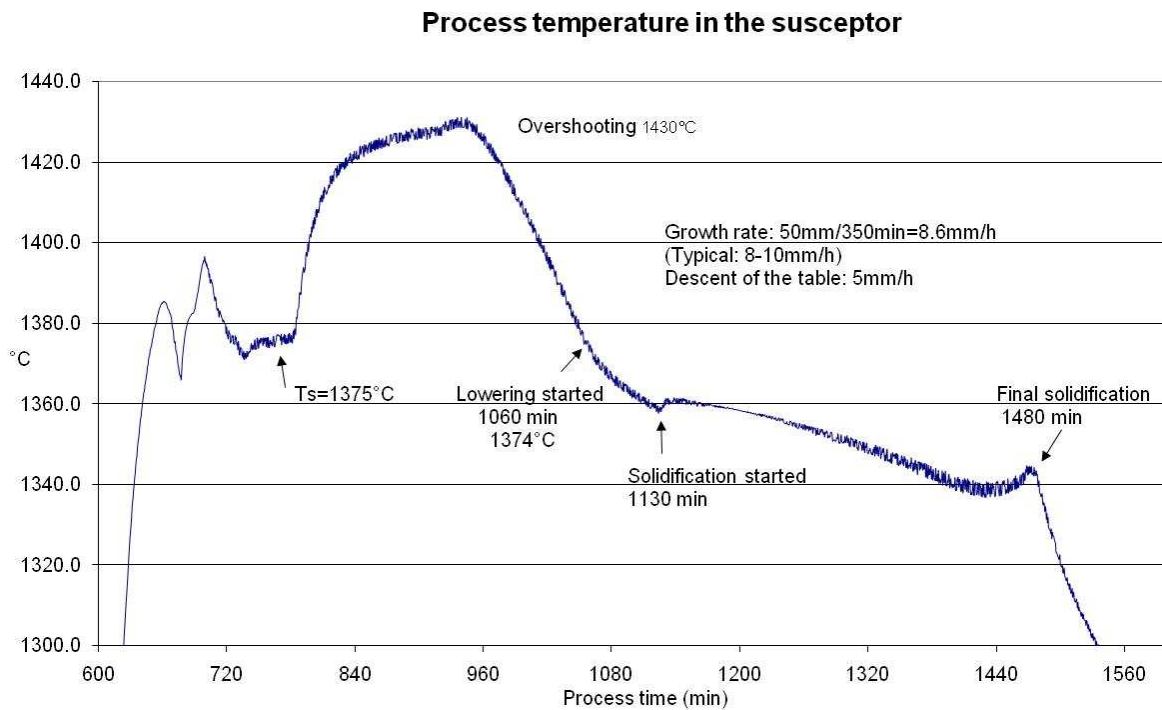


Figure 19: Process of casting of the ingots in Bridgman furnace.

Germanium mass percentage for each sample is shown in Table 1:

	Ge-10	Ge-8	Ge-6	Ge-4	Ge-1	Ge-2	Ge-3
Ge %	3.90E-04	1.55E-03	3.88E-03	1.55E-02	2.59E-02	0.258	1.028

Table 1: Ge concentration in Ge-doped samples.

To investigate the effect of precipitation strengthening method, two additional samples were studied. These two samples, obtained in the same way as the samples described above, were boron doped as well and intentionally alloyed with hafnium. The mass percentage of Hf is shown in Table 2:

	Hf-1	Hf-2
Hf %	6.03	11.48

Table 2: Hafnium concentration in Hf-doped samples.

In addition to all the samples described, one reference sample with no alloying elements was studied in the same way in order to have a comparison. This sample is called *Si-1*.

4.2 Sample preparation

Before doing any measurement by the methods described below, the samples must be polished and then, in case of PV Scan measurements, etched.

4.2.1 Polishing procedure

Samples are mounted on to a planar aluminium plate using a water-soluble wax. Samples are heated to the flow point of the wax (at least 54 °C) then a thin layer of wax is applied and the sample is fitted to a sample holder. To remove the sample after the polishing, it is necessary to reheat it and carefully slide it off from the sample holder. Afterwards, the sample holder is mounted on a support in the polishing machine. This support, located above the polishing disk, applies a constant force at a given rotation speed while the polishing disk rotates at the same speed but in opposite direction.



Figure 20: Drawing of the polishing equipment seen from above (left) and the sample holder seen from the side (right).

The rotation speed used for this work was 300 rpm.

The polishing procedure consists of the following steps:

- two grinding steps with grinding paper with mesh of 500 and 1200, respectively. Three minutes each;
- three polishing steps on polishing pad. Diamond spray size of 9 µm, 3 µm and 1 µm respectively. Three minutes each;
- one step on polishing pad with slurry with silica particle diameter of 50 – 70 nm. One minute;
- one step on polishing pad with water. One minute.

4.2.2 Etching procedure

Samples, which contain dislocations, are placed in an environment capable of removing atoms from the surface. If the rate of atom removal is higher at the dislocations than at the matrix, pits are formed, if the rate is smaller, hillocks are formed. The most common methods for slow and controlled atom removal from crystal surfaces are chemical and electrolytic etching. One group of dislocations etches contains HF, HNO₃ and a diluting agent, such as acetic acid, in different ratios. The basic reaction in the dissolution of a silicon surface is an oxidation of the silicon followed by the removal of the oxide by the HF.

After polishing, the etching procedure consists of the following steps:

- RCA cleaning, step 1. Performed with a 1:1:5 solution of NH₄OH + H₂O₂ + H₂O in order to remove organic contaminants. 10 minutes at 70 °C;
- RCA cleaning, step 2. HF dipping in order to remove thin oxide layer and ionic contaminants. Variable time between 30 seconds and 2 minutes at 25 °C;
- Sopori etching. 20 or 30 seconds at 25 °C;
- RCA cleaning, step 3. Performed with a 1:1:6 solution of HCl + H₂O₂ + H₂O in order to remove the remaining traces of metallic contaminants. 10 minutes at 70 °C.

RCA cleaning is a standard set of wafer cleaning steps which needs to be performed before high temperature processing steps (oxidation, diffusion, CVD) of silicon wafers [29]. Sopori etch consists of hydrofluoric acid (HF), acetic acid (CH₃COOH), and nitric acid (HNO₃) in a volume ratio of 36:20:2 [30]. If Sopori etched samples are analysed by the use of PV-Scan, care must be taken. If Sopori etch used is not fresh, a bluish thin oxide layer may sometimes form on the surface of the sample. This bluish layer might influence the reflection of the laser beam. Another serious problem is when an acid or water droplet sticks to the sample surface after etching and dries there. In this case, spots from the droplets will form on the sample surface and, in measurements with PV-Scan, will be counted as dislocations. To avoid this, the samples can be washed in ethanol before blow-dried [16].

4.3 Fourier Transform Infrared Spectroscopy (FTIR)

FTIR is an analytical technique used to identify the bond concentrations of organic and inorganic species in solids and thin films. This technique measures the absorption of various infrared wavelengths by the species of interests. These infrared absorption bands identify specific molecular components and structures. Infrared radiation is passed through a sample.

Coupling between bonds and radiation appear as absorption peaks in the measured spectrum. For a given sample thickness, the integrated area is often proportional to bond concentration. Bond concentration can either be derived directly from transmittance spectra or modelled towards a set of spectra. The latter method leads to less error on the measurements. In its simplest form, a Fourier transform spectrometer consist of two mirrors located at a right angle to each other and oriented perpendicularly. A beam splitter is placed at the vertex of the right angle and oriented at 45° angle relative to the two mirrors. Radiation incident on the beam splitter is divided into two parts, each of which propagates down one of the two arms and is reflected off one of the mirrors. The two beams are then recombined and transmitted to the detector. By scanning the movable mirror over some distance, an interference pattern is produced that encodes the spectrum of the source [17].

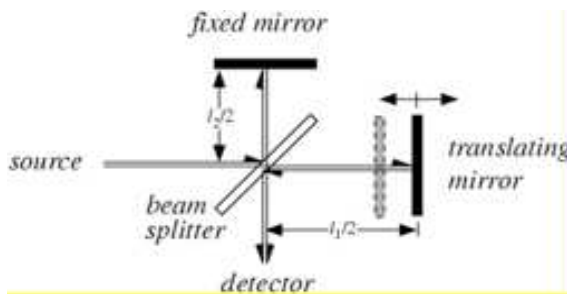


Figure 21: Representation of FTIR equipment.

This equipment leads to an easy, non-destructive measurement that requires samples polished on both sides. It is good for rough estimation of species concentrations but has high uncertainty: the proportionality factors are ambiguous for certain types of species. The equipment used in this work is Nexus 6700 of ThermoScientific.

4.4 Electron Probe Micro Analyser (EPMA)

Electron microscope based technique analyses chemical composition by X-rays emitted when a mechanically polished sample is bombarded with electrons. When highly energetic electrons are used to bombard a sample, secondary electrons are emitted from the inner shells of the atoms. Electrons from higher energy shells will relax to fill the empty position, releasing its excess energy as X-rays characteristic of the transition energy. The fraction of the energy released as X-rays (fluorescence yield) is higher for higher atomic number (Z). Thus, EPMA has higher sensitivity for heavy elements than for light elements. An EPMA system is

equipped with two type of detectors: the Energy Dispersive Spectrometer (EDS) and the Wavelength Dispersive Spectrometer (WDS). These detectors are complementary in the sense that where EDS is fast but has poor sensitivity, WDS is slower but has better sensitivity [18]. The EPMA instrument used in this work was Jeol JXA-8500F. EPMA is a non-destructive technique that allows quantitative analysis. However, in the case of silicon, other materials

may be damaged by the high electron current and low detection limit compared to contamination levels are commonly observed.

4.5 Four-point probe

The resistivity of a semiconductor is an important material requirement and resistivity determination performed during device fabrication is widely used in the industry. The four-point probe method is used and the ASTM standards F43-93 and F723-97 are used for measurement and conversion between resistivity and dopant density. The four-point probe is placed on a flat surface on a specimen which can be approximated as semi-infinite, that means that the thickness of the sample and the distance from any probe point to the nearest edge are at least four times the probe spacing. A direct current is passed through the sample between the two outer probes and the potential difference is measured between the inner probes.

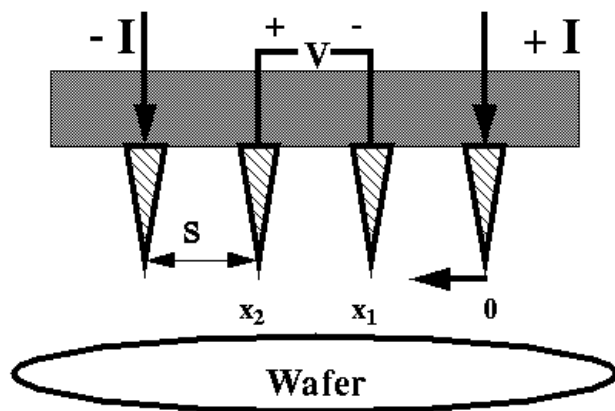


Figure 22: Four-Point probe.

Semiconductors have a significant temperature coefficient and the sample temperature should be known at the time of measuring and the current used should be small to avoid resistivity heating. In case of block measurements, the resistivity, ρ , is calculated by equation 11:

11

$$\rho = \frac{2 \cdot \pi \cdot s \cdot V}{I}$$

where s is the probe spacing, I is the applied current and V is the measured voltage. For wafer measurements:

12

$$\rho = \frac{4.532 \cdot V \cdot t}{I}$$

where t is the thickness of the wafer.

The actual conversion between resistivity and boron concentration is done by using the empirical equation below, where N is the dopant density given in cm^{-3} and ρ is the resistivity given in Ωcm [19, 20]:

13

$$N = \frac{1.33 \cdot 10^{16}}{\rho} + \frac{1.082 \cdot 10^{17}}{\rho \cdot [1 + (54.56 \cdot \rho)^{1.105}]}$$

The probe used for this work has pin spacing of 0.635 mm.

4.6 Optical scanner and Intercept method

The use of an optical scanner allows to get an image of a silicon wafer as polished or after etching to reveal grain boundaries. A scanner is a device that optically scans images, printed texts, handwritings or objects and converts them to a digital image. Currently available scanner typically use Charge-Coupled Device (CCD) or Contact Image Sensor (CIS) as the image sensor. A connection to a computer is needed for image analysis and storage. The image size is dependent to the standard of compression used: a TIF file for a 5x5 cm wafer at full resolution will be 788 MB and a JPEG will be about 80 MB. The images used in this work has resolution of 600 dpi and were taken with scanner CANON CanoScan8800F.

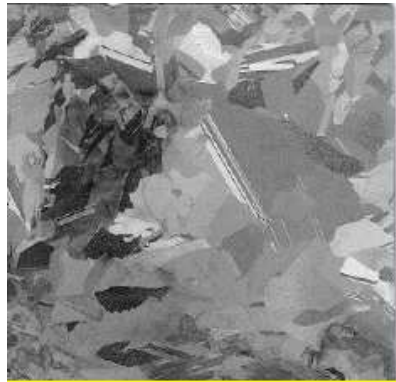


Figure 23: Example of an image of a scanned wafer.

Optical scanner is a very common, easy-to-use and cheap instrument that can reveal crystal morphology. Moreover, the measurements are limited because quantitative analysis is not possible and the resolution approaches what is possible with light. Grain size is a very difficult parameter to measure. In case of columnar grains, the simplest method is to mark any number of equally spaced lines perpendicular to the grain growth direction and count the number of grain boundaries crossing each line. The results consist of values for the total line length L , the total number of intersections n_i and the mean linear intercept length l , given by equation 14 [21]:

$$14 \quad l = \frac{L}{n_i}$$

This definition does not consider the varying properties of the grain boundaries. In areas of multiple twins, the grain size will become very small and very difficult to measure using this method.

4.7 PV Scan

PVScan is an apparatus that permits the measurement of dislocation density based on scattered light from an etched wafer surface. A laser illuminates the sample perpendicularly. Light is scattered by the etch pits and the diffuse light is collected by an integrating sphere. The signal is directly proportional to the etch pit density which is interpreted as the dislocation density. Light hitting a spherical dislocation etch pit will be high angle scattered or scattered diffused, while light scattered from a v-shaped groove originated from a grain boundary will be low angle scattered. Low angle scattered light is collected by another

detector, so dislocations and grain boundaries can be distinguished and measured separately and simultaneously. In case of one grain boundary in a dislocated area the error is negligible but, in the case of multiple twins, serious errors may occur. It is shown that twins located close to each other will cause an interference pattern which scatters light with a high angle in certain directions, creating an arc of 180° to the wafer surface. This light will be detected by integrated sphere detector and twins will thus be measured as dislocations [22].

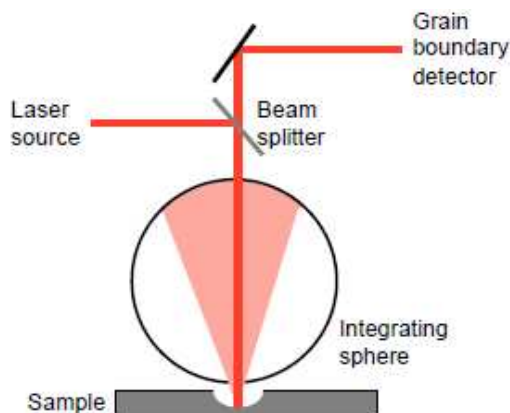


Figure 24: Diffuse scattering from a spherical dislocation etch pit.

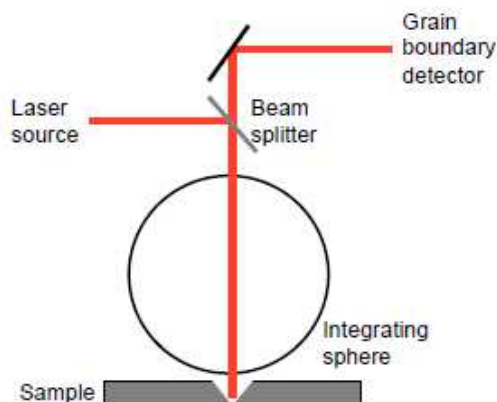


Figure 25: low angle scattering from a v-shaped groove originating from a grain boundary.

PV Scan is a fast measurement and the only available method that may provide statistical measurements on large scale samples. On the other hand, statistical measurements will be affected by errors if scanned areas contain multiple twins. Sample preparation consist of grinding, polishing and etching. Equipment used is PV-Scan 6000 of GT Solar Technologies. In this work an area of 7×7 cm was scanned with a resolution of $50 \mu\text{m}$. The software connected to PV-Scan generates a matrix of 1400×1400 values. Each value is the defect

density of an area of $50 \times 50 \mu\text{m}$ in the sample. These results can be plotted in a histogram in order to show the defect density distribution. More resolution in the representation can be obtained by reducing the width of the intervals in the histogram. Finally, in order to have a better understanding of the results, a curve is drawn connecting the central value for each interval of the histogram. Resulting graphs are shown in Figure 38 and 42.

5 Results and discussion

5.1 Distribution of alloying elements

EPMA measurements shows the distribution of the alloying elements, such as Ge and Hf, throughout the samples. Missing values in the following graphs are due to the low detection limit of the probe. Scheil equations describe solute distribution during solidification of an alloy by assuming a local equilibrium of the solidification front at the solid-liquid interface. The concentration of the solute in the liquid during solidification is:

$$15 \quad C_L = C_0 \cdot (f_L)^{k-1}$$

While, the concentration of the solute in the solid is:

$$16 \quad C_s = k \cdot C_0 \cdot (1-f_s)^{k-1}$$

Where k is the partition coefficient determined from the phase diagram, C_0 is the initial concentration of the solute, f_L the fraction of liquid and f_s the fraction of solid. Hence, if k is less than 1, the concentration of solute during solidification is higher in the liquid fraction and there will be an accumulation of solute in the part that solidifies last. On the other hand, if k is larger than one, the solute will accumulate in the part that solidifies first. Figures 26, 27, 28 show the germanium distribution in each sample measured by EPMA. The y-axis is represents the germanium mass percent and the x-axis, f_s , represents the fraction of solid of the sample: at the bottom f_s is 0, at the top f_s is 1. A best fitting of these results was made using equation 16: k has been imposed equal to 0.33. In Figure 26 it is possible to see that a small amount of measured values is present for each sample: it is because the Ge concentration in these samples is very low and the low detection limit of the EPMA does not allow a precise measurement. That also explain because the values measured in these samples does not fit well the Scheil's equation curves.

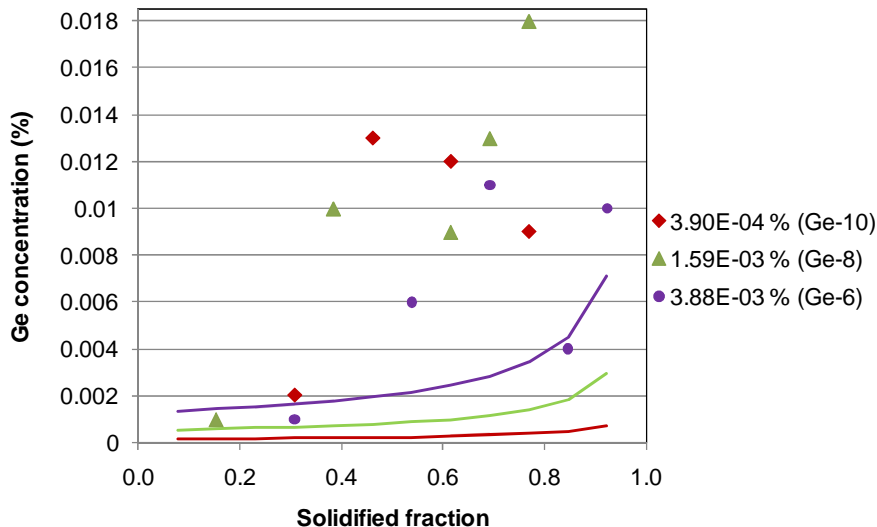


Figure 26: Germanium distribution of Ge-doped samples with lowest concentration (Ge-6, -8,-10).

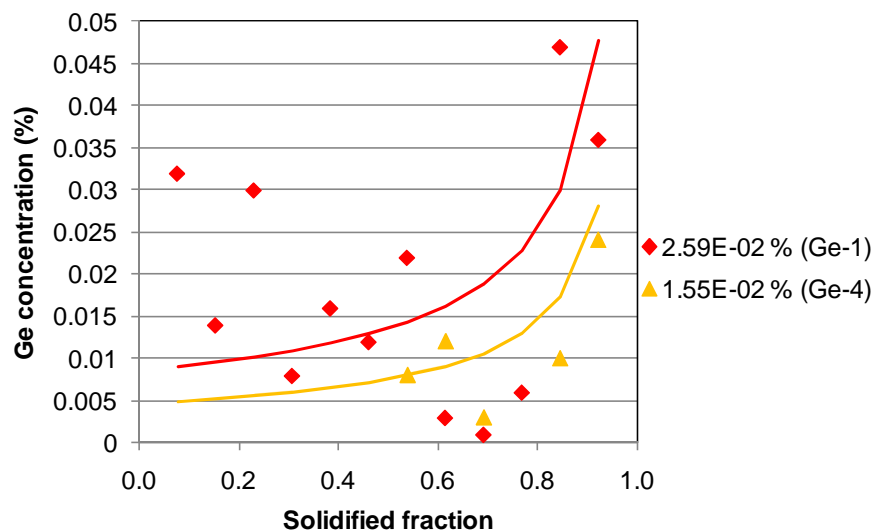


Figure 27: Germanium distribution of Ge-doped samples with medium concentration (Ge-1, -4).

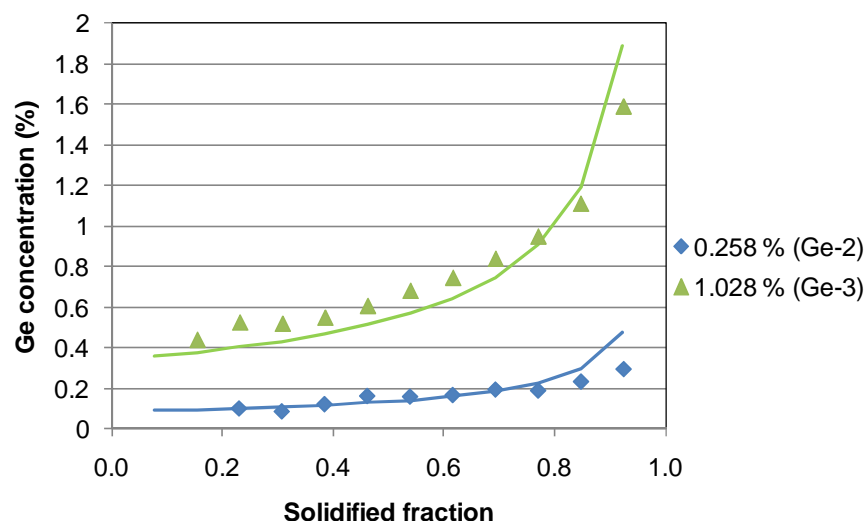


Figure 28: Germanium distribution of Ge-doped samples with highest concentration (Ge-2, -3).

As shown in Figure 27 and 28, Scheil's equation curves fit very well the measurement for the highest concentration of Ge (samples named Ge-1, -2, -3, -4).

Results for the Hf-doped samples are shown in Figure 29:

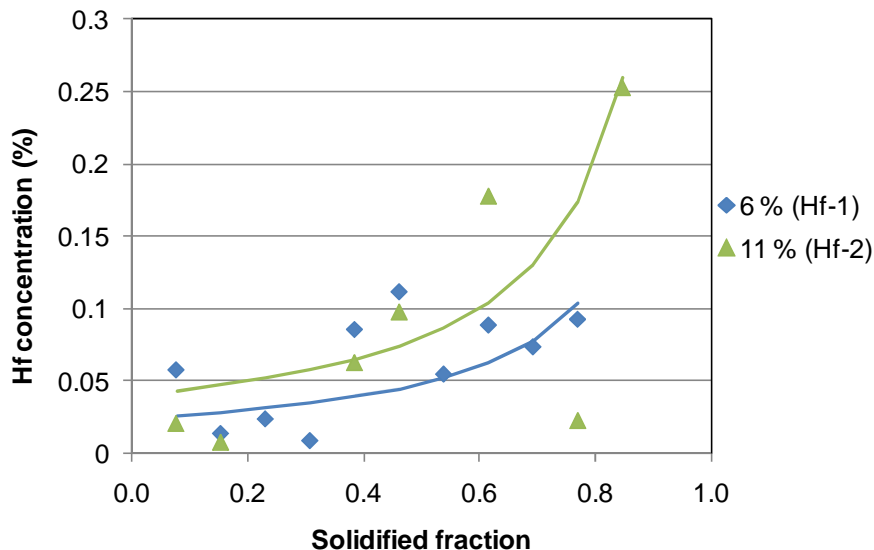


Figure 29: Hafnium distribution of Hf-doped samples.

The equilibrium distribution coefficient of Hf in silicon is not known. However, it is possible to say that is less than 1, as the concentration of Hf increases from bottom to top and as it can be seen from the Hf-Si phase diagram (see Figure 17, page 35). By making a fitting of these results with equation 16, it was found that the value for k that best approximates the results is 0.004.

5.2 Oxygen and Carbon distribution

FTIR measurements were conducted by recording the absorbance spectrum every 4 mm from the bottom to the top of the sample. The spectrum had two peaks representative of oxygen and carbon concentration. The oxygen peak was at 1107 cm^{-1} and the carbon peak at 605 cm^{-1} . The absorption was converted into concentration in atoms/cm³ by the conversion coefficient implemented in the software used.

Results for Ge-doped samples are shown in Figure 30 and 31:

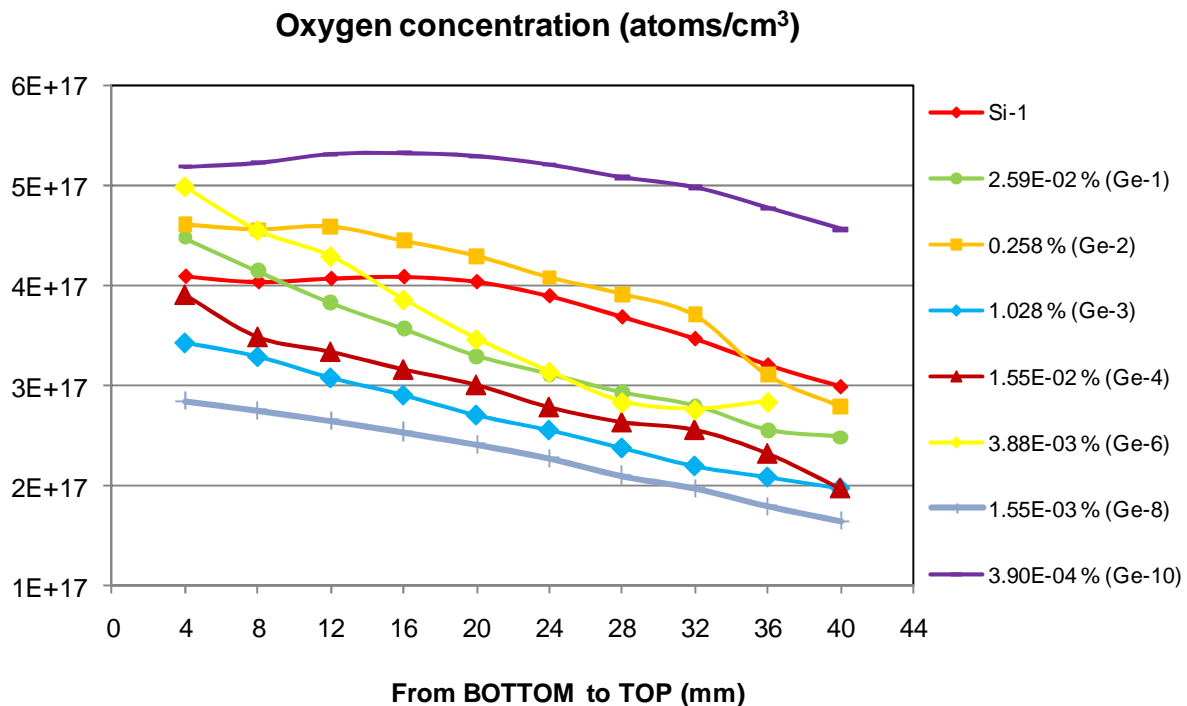


Figure 30: Oxygen concentration in Ge-doped samples.

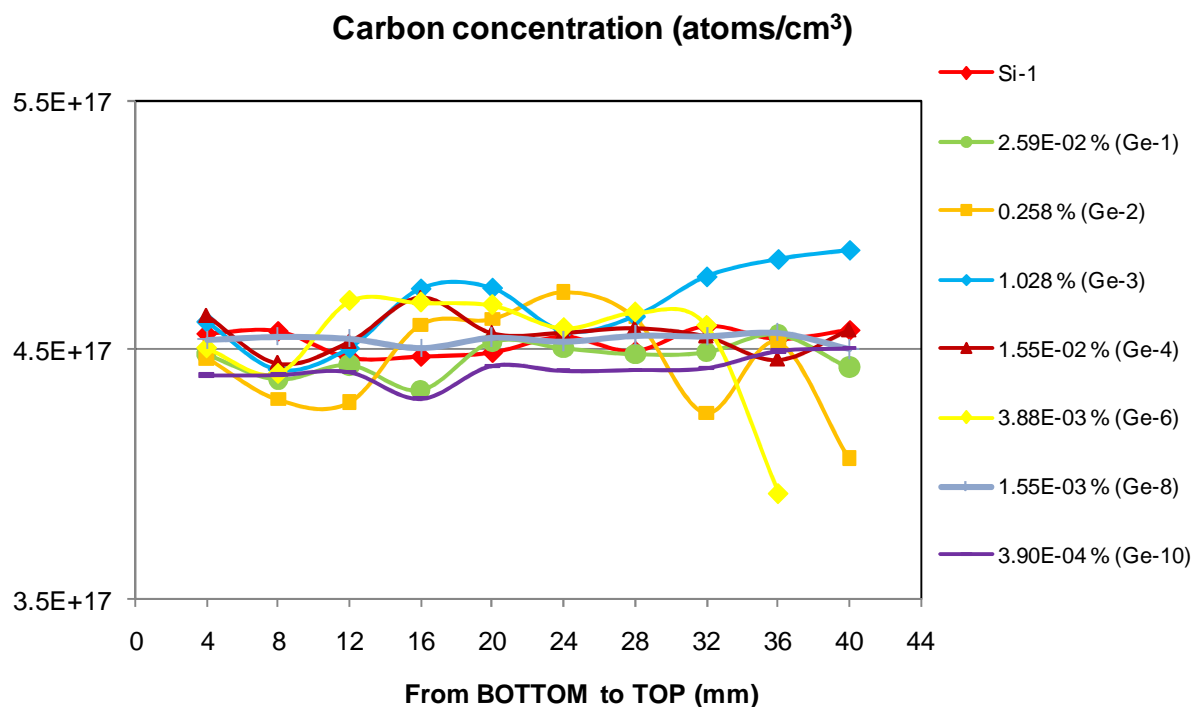


Figure 31: Carbon concentration in Ge-doped samples.

The same measurements were taken for the two Hf-doped samples but, in the case of the sample with the highest Hf concentration (Hf-2), the spectrum was disturbed and the peaks were not distinguishable. It is possible to argue that this disturbance was due to the precipitates distributed throughout all the sample as can be seen in Figure 52 (Appendix A).

Results for the Hf-1 sample are shown in Figures 32 and 33:

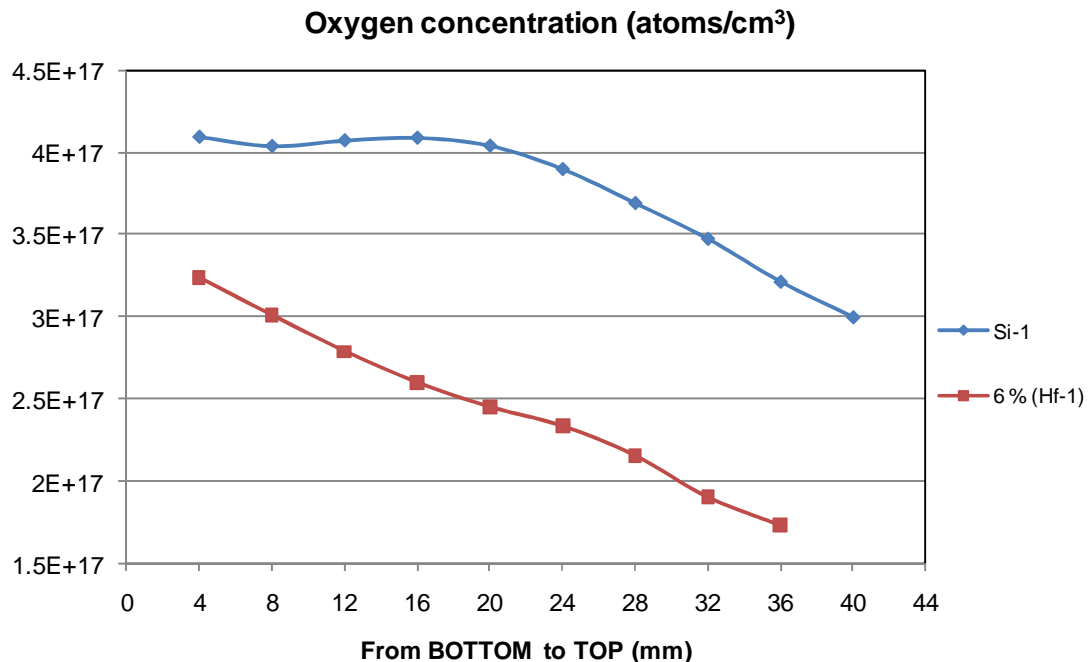


Figure 32: Oxygen concentration in Hf-doped sample.

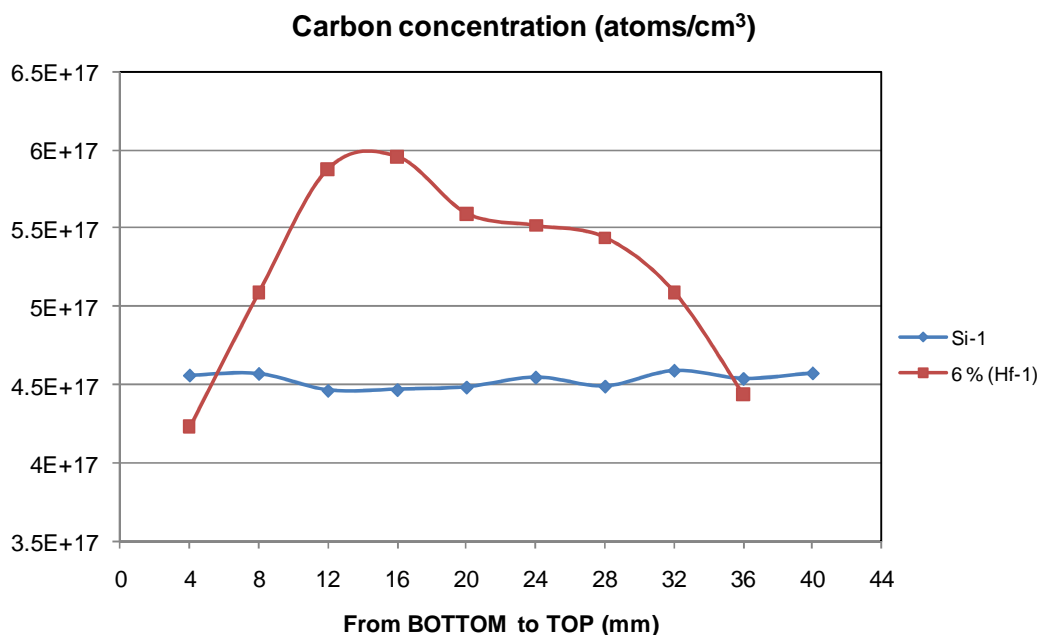


Figure 33: Carbon concentration in Hf-doped sample.

These measurements were focused on identifying whether the factors normally involved in a casting process, as the concentration of oxygen and carbon, could change their behaviour within the ingots containing germanium. As shown in Figure 30, the oxygen content tends to decrease from bottom to top as expected, since the partition coefficient for oxygen in silicon (considering the evaporation in the melt) is considered equal to 1.4 [26]. Figure 31 shows the values of carbon concentration in Ge-doped samples. It seems that carbon concentration from bottom to top is almost constant but it can be expected that in the upper part of the ingot the content of carbon increases exponentially since the partition coefficient of carbon in silicon is 0.07 [27]. However, measurements on the top of the samples are very difficult because the spectrum of FTIR measurement is disturbed. Oxygen distribution in Hf-doped sample (Figure 32) follow the same trend as described above, decreasing from bottom to top. Measurements of carbon concentration in Hf-doped sample (Figure 33) show an increase in the central part of the sample followed by a sudden decrease moving to the upper part. It is possible to argue that this trend is mostly due to the large presence of precipitates that negatively affect the measurement (Figure 51, Appendix A). Through these observation, it is possible to see that there is no influence of Ge and Hf in the distribution of oxygen and carbon in the ingot.

5.3 Resistivity

Resistivity measurements could vary if the probe is positioned within the grain or across a grain boundary and thus the results plotted below are an exponential fitting of individual measurement made from the bottom to the top of each sample. The equation used for the fitting is of the form $y = a \cdot e^{bx}$.

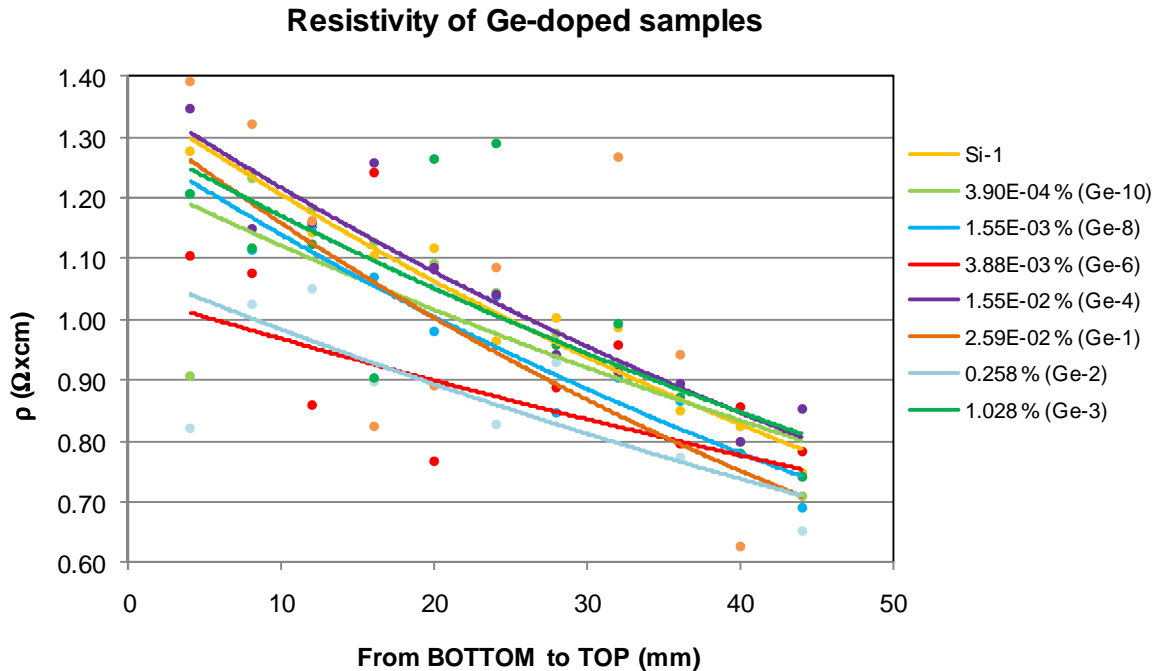


Figure 34: Resistivity trend of Ge-doped samples.

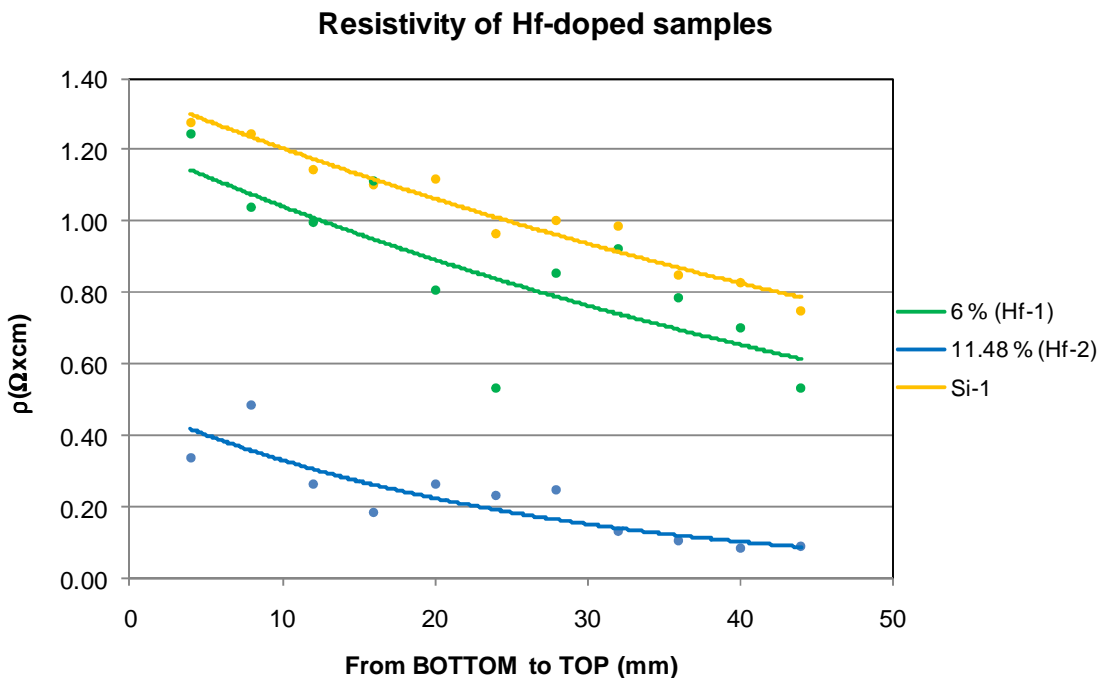


Figure 35: Resistivity trend of Hf-doped samples.

In both Ge- and Hf-doped samples, it is possible to see a decrease of resistivity due to increase of boron content on the top of the ingot. This behaviour is explained by equation 13: if the dopant density increases, the resistivity decreases. It was observed that the mean value of resistivity does not change, remaining constant at about $10 \Omega\text{mm}$. An exception was detected in the sample with the highest concentration of Hf: its mean value of resistivity was about $2.5 \Omega\text{mm}$.

5.4 Grain size measurements

Each sample has been scanned by the optical scanner and 5 mm spaced lines have been drawn on the image of the sample from the bottom to the top. By counting the number of interception of grain boundaries with these lines, Mean Linear Intercept Length values were obtained. The correlation coefficient of linear fitting of Mean Linear Intercept Lengths values was 0.25 and thus insufficient to affirm any correlation between grain size and Ge concentration.

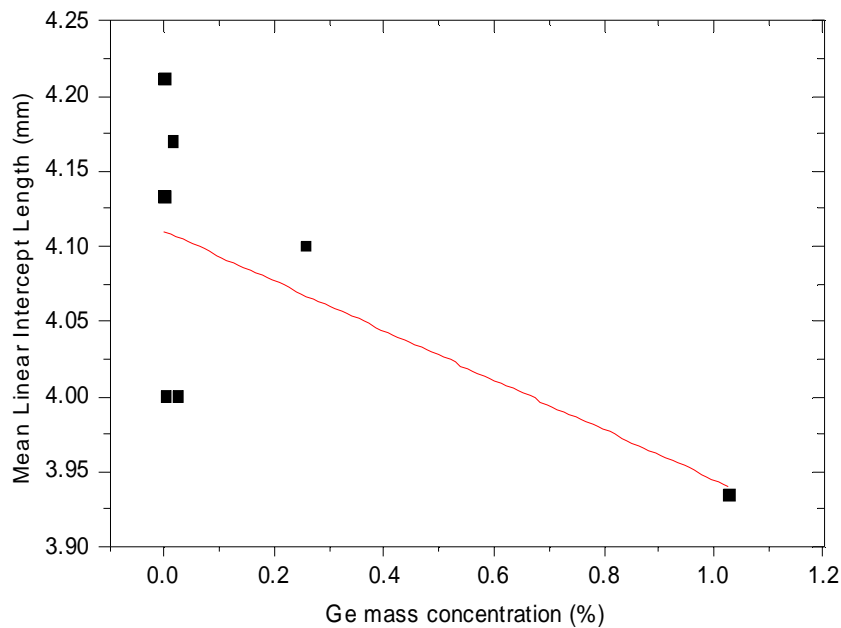


Figure 36: Mean Linear Intercept Length values for Ge-doped samples with linear fitting (red).

Same measurements have been tried in Hf-doped samples but it was difficult to measure the grain size with this method because of visible precipitates throughout all the highest part for more than a half of the entire surface.

5.5 Dislocation density

To get results about dislocation density with PV-Scan, an area of 5x3.5 cm in each sample was measured, while the outer edges of the samples, where there is an accumulation of defects, were excluded. Figure 37 shows how the area was chosen for the measurement:

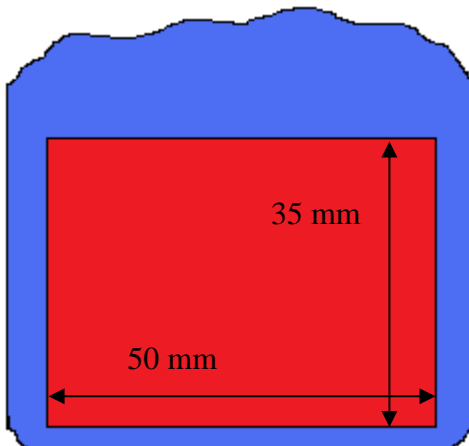


Figure 37: Sketch of the scanned area on the sample.

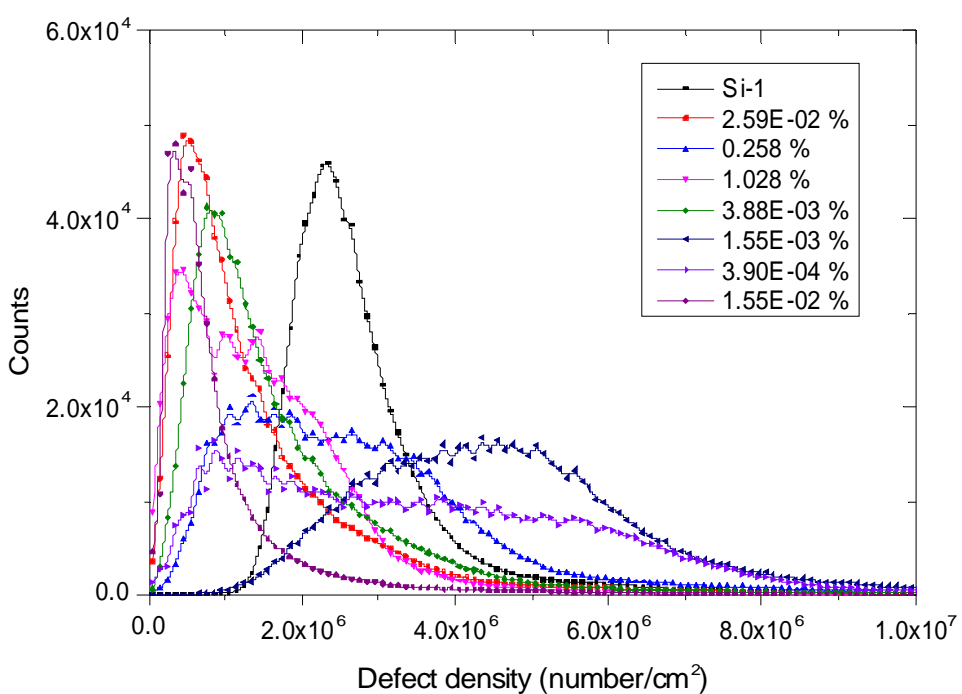


Figure 38: Defect density distribution on Ge-doped samples.

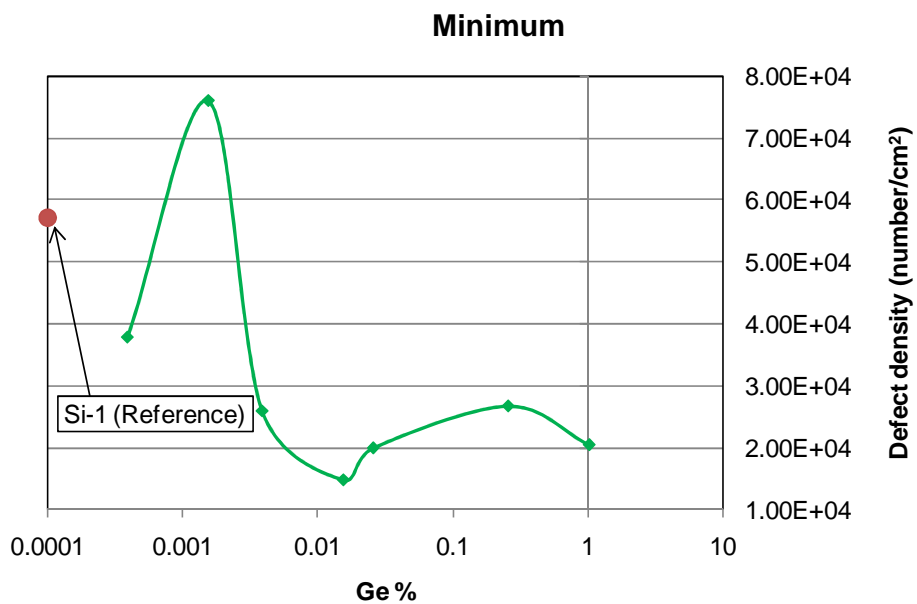


Figure 39: Minimum values for dislocation density in Ge-doped samples.

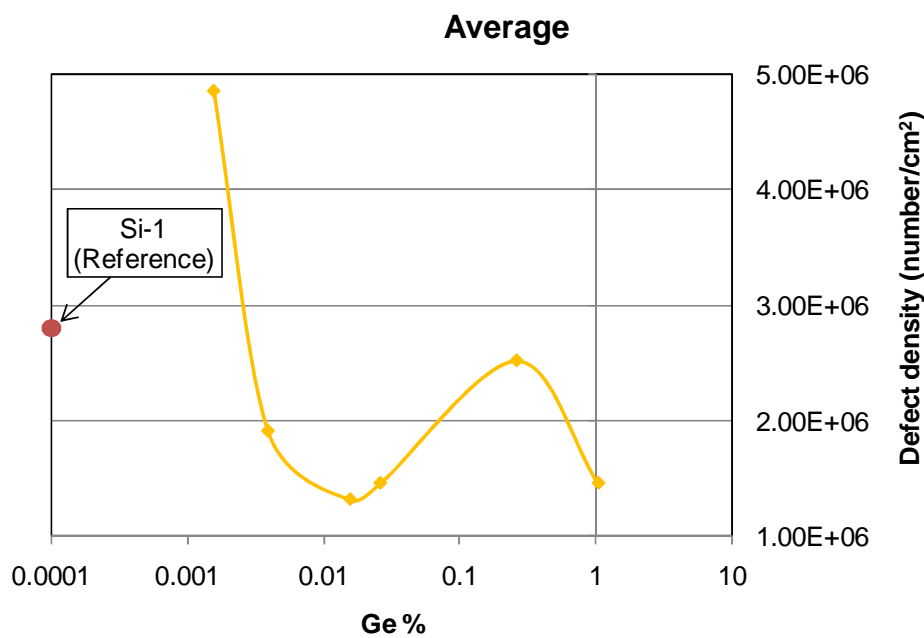


Figure 40: Average values of dislocation density in Ge-doped samples.

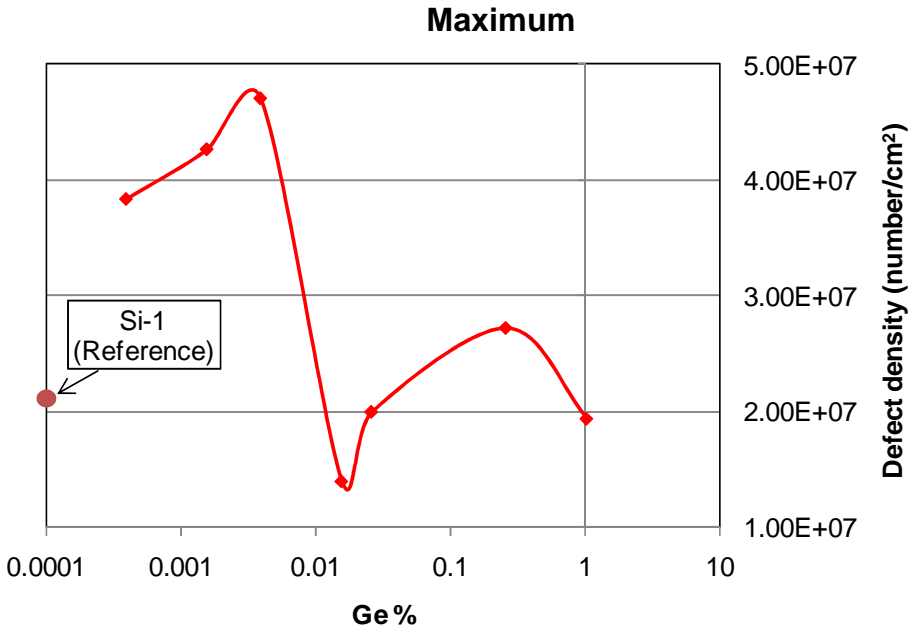


Figure 41: Maximum values of dislocation density in Ge-doped samples.

PV Scan measurements may reveal an influence of germanium doping. In Figure 38 the counts of points with a certain value of dislocation density are presented. As can be seen, the majority of the samples shows a lower value for the peak of the curve: it means that, compared to the reference sample (Si-1), there is a decrease on dislocation density with increasing Ge content. The three plotted curves for the two samples with the lowest Ge concentration and 0.258 % of Ge do not have the same trend. It is possible that these three measurement were influenced by the large presence of twins throughout the sample (Figure 45, 49, 50 in Appendix A): PVScan detects the twins as dislocations. Omitting these three curves, it can be observed that the lowest dislocation density is reached by the sample with Ge concentration of 0.0155% of weight. This result can also be continued by observing the curves related to the minimum, the average and the maximum values of dislocation density for each sample (Figure 39, 40, 41, respectively): in each graph, the lowest value is reached by the sample with 0.0155% of Ge. Hence, it is possible that the best effect on dislocation density is shown by the sample with Ge concentration of 0.0155 %. However, this result should be taken with caution because previous studies have shown that germanium may have an adverse effect on the main electrical performances of silicon. Ulyashin et al. [23] studied different mono-crystalline Si-Ge alloys with Ge concentration from 2 up to 7 % and showed that the minority carrier lifetimes drastically decrease as the Ge content increases.

Furthermore, it was demonstrated that the traditional treatments for the improvement of this performance were not as efficient as for pure silicon. Germanium concentrations in this work are much lower than those relating to the study of Ulyashin et al. and it should therefore be investigated if the electrical performance is affected in the same way. Measurements with PV-Scan were also conducted on samples doped with hafnium but in this case, the results obtained, while apparently successful (Figure 42), were highly distorted by the massive presence of precipitates which are measured as dislocations (Figure 51, 52 in Appendix A).

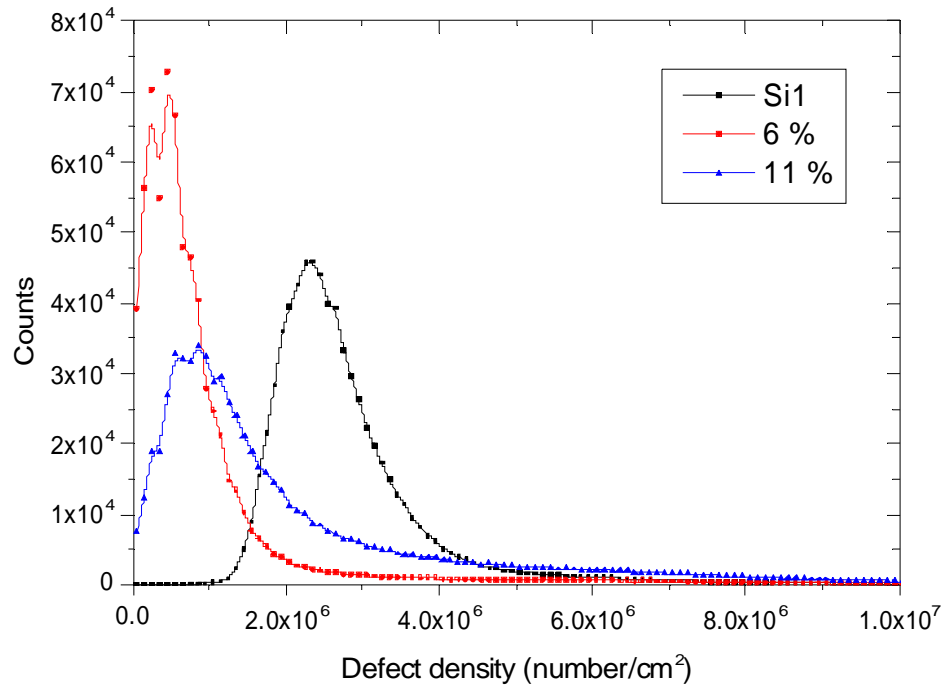


Figure 42: Defect density distribution on Hf-doped samples.

6 Conclusions and further works

6.1 Effect of Ge

- The main result obtained from this work is that germanium in certain concentrations reduces the dislocation density in multicrystalline silicon. Results show that, in addition to a reduction of the average density of dislocation, there is a reduction of maximum and minimum values. The best effect is reached with a germanium concentration of 0.0155% of weight.
- Low concentrations of germanium (less than 1%) seem to positively influence the structural properties of multi-crystalline silicon but the influence on the main electrical properties is not known.
- Acknowledgement of twinned areas is needed to remove their contribution to the measurements and focus the results on dislocation density.
- To determine whether doping with germanium leads to a real increase in efficiency, detailed measurements on the minority carrier lifetime are needed;
- To get better understanding of the effect of germanium on grain size and on dislocation density, it will be necessary to investigate more Ge-doped cast ingot with Ge concentration between 0.01% and 1% of weight.

6.2 Effect of Hf

- It was found that the equilibrium distribution coefficient for Hf in Si is less than 1 and may have a value close to 0.004.
- The main result obtained by studying Hf-doped samples is a decrease of resistivity.
- Measurements on grain size and on dislocation density are difficult if the surface of the sample is highly covered by precipitates.
- Methods to eliminate measurement errors due to the presence of precipitates can be studied.
- To limit the presence of precipitates, samples with less concentration of Hf may be studied, and thus determine if structural and electrical properties can really be influenced by doping with this element.

7 References

- [1] Solar Outlook, September 2005, Navigant Consulting, Inc., San Francisco.
- [2] European Commission, *A strategic research agenda for photovoltaic solar energy technology*, 2007, ISBN 978-92-79-05523-2.
- [3] Images from <http://domymaths.co.uk/structure.htm>.
- [4] Birgit Ryningen, *Formation and growth of crystal defects in directionally solidified multicrystalline silicon for solar cells*. Doctoral thesis at NTNU, 2008, pp. 17-18.
- [5] Flemmings, M. C., Solidification Processing, 1974, McGraw-Hill, Inc., p.3.
- [6] Birgit Ryningen, *Formation and growth of crystal defects in directionally solidified multicrystalline silicon for solar cells*. Doctoral thesis at NTNU, 2008, p. 22.
- [7] Stokkan, Gaute, *Characterization of multicrystalline silicon solar cells, Development of characterization method for the combined effect of dislocations and grain boundaries on the minority carrier lifetime*, 2004, NTNU: Trondheim.
- [8] O'Mara, W. C., R. B. Herring, L. P. Hunt, *Handbook on semiconductor silicon technology*, William Andrew Publishing/Noyes. 2002: 795.
- [9] Birgit Ryningen, *Formation and growth of crystal defects in directionally solidified multicrystalline silicon for solar cells*. Doctoral thesis at NTNU, 2008, p. 25-26.
- [10] Y. Nishino and T. Imura, *Generation process of dislocations in precipitate-containing silicon crystals*, phys. stat. Sol. (a) 73, 173-182 (1982).
- [11] F. Barbe, S. Forest and G. Cailletaud, *Intergranular and intragranular behaviour of polycrystalline aggregates, Part 2: Results*, International Journal of Plasticity 17, 2001, 537-563.
- [12] H. Gleiter, S. Mahajan, K. J. Bachmann, *The generation of lattice dislocations by migrating boundaries*, Acta Metallurgica Inc., Vol. 28, 1980, p. 1603.
- [13] Birgit Ryningen, *Formation and growth of crystal defects in directionally solidified multicrystalline silicon for solar cells*. Doctoral thesis at NTNU, 2008, p. 42-43.
- [14] Daniel MacDonald, L. J. Geerligs, *Recombination activity of interstitial iron and other transition metal point defects in p- and n-type crystalline silicon*, Applied Physics letters, Volume 85, Number 18, November 2004, pages 4061-4063.
- [15] M. P. Bellmann, *How to inhibit dislocation multiplication in multi-crystalline silicon?*, Scientific Group Seminar (Edsåsdalen, Sweden), NTNU, 2008.

- [16] Birgit Ryningen, *Formation and growth of crystal defects in directionally solidified multicrystalline silicon for solar cells*. Doctoral thesis at NTNU, 2008, p. 36-38.
- [17] R. J. Bell, *Introductory Fourier Transform Spectroscopy*. New York: Academic Press, 1972.
- [18] Dieter K. Schroder, *Semiconductor Material and Device Characterisation*, 3rd edition ISBN 0-471-73906-5, pp 639.
- [19] *The American Society for Testing and Materials (ASTM) Standard Test Methods for Resistivity of Semiconductor Materials*, F 43-93 (1993).
- [20] *The American Society for Testing and Materials (ASTM) Standard Practice for Conversion Between Resistivity and Dopant Density for Boron-Doped, Phosphorus-Doped, and Arsenic-Doped Silicon*, F 723-97 (1997).
- [21] L. J. M. G. Dortmans, R. Morrell, G. de With, *Round robin on grain size measurement for advanced technical ceramics*, Journal of the European Ceramic Society, Number 12, 1993, pages 205-213.
- [22] G. Stokkan, “*Characterisation of dislocation density of multicrystalline silicon wafers using the PVScan 6000*”, 22nd European Photovoltaic Solar Energy Conference (WIP-Renewable Energies, Milan, Italy, 2007).
- [23] A. G. Ulyashin et al., *Ge composition dependence of the minority carrier lifetime in monocrystalline alloys of $Si_{1-x}Ge_x$* , Materials Science in Semiconductor Processing, Number 9, 2006, pages 772-776.
- [24] Erofeev, Nikitenko, *Mobility of dislocations in silicon containing substitutional and interstitial impurities*, Fiz Tverd Tela, Vol. 13, 1971
- [25] Trumbore, F. A., Bell Syst. Tech. J. 39, 1960, 205.
- [26] Nozaki T., Yatsurugi Y., Akiyama N., Endo Y., Makide Y., *Radioanal. Chem.* 19, 1974, 109.
- [27] Nozaki T., Yatsurugi Y., Akiyama N., Endo Y., *J. Electrochem. Soc.* 117, 1970, 1566.
- [28] Callister, William D. Jr., *Fundamentals of Materials Science and Engineering*, John Wiley & Sons, Inc. Danvers, MA., 2005.
- [29] W. Kern, *Handbook of Semiconductor Wafer Cleaning Technology*, Applied Science Technology, William Andrews Publishers, pp. 519-526, 1993.
- [30] B. L. Sopori, *Broadband very low reflectance surface*, Applied Optics, Volume 27, Number 1, p. 25, 1988.
- [31] A. Müller, P. M. Nasch, *RE-Si-CLE: Recycling of silicon rejects from PV production cycle*, NET Nowak Energie & Technologie AG, Annual report, 2003.

- [32] E. Bombach, A. Müller, K. Wambach, I. Röver, *Recycling of solar cells and modules – Recent improvements*, 2005.
- [33] A. K. Søiland, *Silicon for solar cells*, Department of Materials Technology, NTNU, Trondheim 2004.
- [34] Schei, Tuset, Tveit, *Production of High Silicon Alloys*, Tapir Forlag, 1998, chapter 3.
- [35] J. Weis, N. Auner, *Organosilicon Chemistry V: From molecules to materials*, Wiley and Sons, 2003, p.501.
- [36] M. de Wild-Schot, E. Alsema, *Towards cleaner solar PV environmental and health impacts of crystalline silicon photovoltaics*, Volume 5, 2004, p. 46-49.
- [37] R. M. Swanson, *A vision for crystalline silicon photovoltaics*, Prog. Photovolt, 2006, 14:443-453.
- [38] Birgit Ryningen, *Formation and growth of crystal defects in directionally solidified multicrystalline silicon for solar cells*. Doctoral thesis at NTNU, 2008, p. 7-8.
- [39] A. F. B. Braga, S. P. Moreira, P. R. Zampieri, J. M. G. Bacchin, P. R. Mei, *New processes for the production of solar-grade polycrystalline silicon: a review*, Solar Energy Materials and Solar Cells 92, 2008, p. 418-424.
- [40] Janine Friedl, *The role of oxygen in multicrystalline silicon*, NTNU Project work (TMT 4500), Trondheim, 2009, p.17.
- [41] K. Peter et al., *Analysis of multicrystalline solar cells from solar grade silicon feedstock*, 31st IEEE PVSC Florida, 2005.
- [42] Janine Friedl, *The role of oxygen in multicrystalline silicon*, NTNU Project work (TMT 4500), Trondheim, 2009, p.18.
- [43] B. Ceccaroli, K. Friestad, *Refining of metallurgical grade silicon*, United States, Patent 6,861,040, March 2005.
- [44] C. Zahedi, E. Enebakk, K. Friestad, M. G. Dolmen, J. Heide, T. Buseth, R. Tronstad, C. Dethloff, *Solar grade silicon from metallurgical route*, Technical Digest of the PVSEC-14 Bangkok, 2004.
- [45] A. Müller, K. Wambach, E. Alsema, Life cycle analisys of a solar module recycling process, Materials Research Society Symposium Proceedings, 2006, vol. 895, p.89-94.
- [46] L. J. Geerligs, G. P. Wyers, R. Jensen, O. Raaness, A. N. Wærnes, S. Santén, A. Reinink, B. Wiersma, *Solar-grade silicon by a direct route based on carbothermic reduction of silica: requirements and production technology*, Energy research Centre of the Netherlands (ECN), 2002.
- [47] Birgit Ryningen, *Formation and growth of crystal defects in directionally solidified*

- multicrystalline silicon for solar cells.* Doctoral thesis at NTNU, 2008, p. 12-13.
- [48] H. R. Huff, T. G. Digges, O. B. Cecil, *Distribution coefficient of boron and phosphorous in silicon*, J. Appl. Phys. 42, 1235, 1971.
- [49] M. C. Flemmings, Solidification processing, 1974, McGraw-Hill Inc. 363.
- [50] Birgit Ryningen, *Formation and growth of crystal defects in directionally solidified multicrystalline silicon for solar cells.* Doctoral thesis at NTNU, 2008, p. 10.
- [51] J. A. Burton, E. D. Kolb, W. P. Slichter, J. D. Struthers, *The distribution of solute in crystals grown from the melt. Part II. Experimental*, Journal of Chemical Physics (1953), Vol. 21, p. 1953-1991.
- [52] Birgit Ryningen, *Formation and growth of crystal defects in directionally solidified multicrystalline silicon for solar cells.* Doctoral thesis at NTNU, 2008, p. 11.

8 Appendix A

Figures



Figure 43: Si-1.



Figure 44: Ge-1.



Figure 45: Ge-2.



Figure 46: Ge-3.



Figure 47: Ge-4.



Figure 48: Ge-6.



Figure 49: Ge-8.



Figure 50: Ge-10.



Figure 51: Hf-1.



Figure 52: Hf-2.

Tables

Designation	Explanation	Bulk Si (g)	Mass Doping (g)			Total mass (g)
			Boron	Ge	Hf	
Si-1	Reference	320.5	0.0506	0	0	320.5506
Ge-1	Ge-doped	320.7	0.0508	0.0839	0	320.8347
Ge-10	Ge-doped	320	0.0503	0.0012	0	320.0515
Ge-8	Ge-doped	320.1	0.0501	0.0049	0	320.155
Ge-6	Ge-doped	320.9	0.0507	0.0127	0	320.9634
Ge-4	Ge-doped	320.4	0.0503	0.0497	0	320.5
Ge-2	Ge-doped	322.8	0.0507	0.8206	0	323.6713
Ge-3	Ge-doped	321.8	0.0502	3.312	0	325.1622
Hf-1	Hf-doped	315.3	0.0503	0	20.3012	335.6515
Hf-2	Hf-doped	313.4	0.0504	0	40.59	354.0404

Table 3: Composition of the samples. It is shown the Boron, Germanium and Hafnium content.

Height	Ge concentration (%)							Hf concentration (%)	
	Ge-1	Ge-2	Ge-3	Ge-4	Ge-6	Ge-8	Ge-10	Hf-1	Hf-2
5	0.032	//	//	//	//	//	//	0.058	0.021
10	0.014	//	0.441	//	//	0.001	//	0.014	0.008
15	0.03	0.105	0.526	//	//	//	//	0.024	//
20	0.008	0.09	0.52	//	0.001	//	0.002	0.009	//
25	0.016	0.126	0.55	//	//	0.01	//	0.086	0.063
30	0.012	0.166	0.607	//	//	//	0.013	0.112	0.098
35	0.022	0.163	0.682	0.008	0.006	//	//	0.055	//
40	0.003	0.171	0.745	0.012	//	0.009	0.012	0.089	0.178
45	0.001	0.198	0.839	0.003	0.011	0.013	//	0.074	//
50	0.006	0.193	0.948	//	//	0.018	0.009	0.093	0.023
55	0.047	0.237	1.109	0.01	0.004	//	//	//	0.253
60	0.036	0.298	1.586	0.024	0.01	//	//	//	//
65	0.046	0.42	5.423	0.156	0.007	//	//	//	//

Table 4: EPMA measurements on Ge- and Hf-doped samples.

Height (mm)	4	8	12	16	20	24	28	32	36	40
Si-1	4.10E+17	4.04E+17	4.07E+17	4.09E+17	4.04E+17	3.90E+17	3.69E+17	3.47E+17	3.21E+17	3.00E+17
Ge-1	4.47E+17	4.14E+17	3.83E+17	3.57E+17	3.30E+17	3.11E+17	2.93E+17	2.80E+17	2.55E+17	2.48E+17
Ge-2	4.60E+17	4.56E+17	4.58E+17	4.44E+17	4.29E+17	4.08E+17	3.92E+17	3.70E+17	3.11E+17	2.80E+17
Ge-3	3.42E+17	3.29E+17	3.08E+17	2.91E+17	2.71E+17	2.56E+17	2.38E+17	2.20E+17	2.09E+17	1.98E+17
Ge-4	3.91E+17	3.49E+17	3.34E+17	3.17E+17	3.01E+17	2.79E+17	2.64E+17	2.57E+17	2.33E+17	1.98E+17
Ge-6	4.98E+17	4.55E+17	4.29E+17	3.86E+17	3.47E+17	3.14E+17	2.84E+17	2.77E+17	2.84E+17	//
Ge-8	2.85E+17	2.76E+17	2.66E+17	2.54E+17	2.42E+17	2.28E+17	2.10E+17	1.98E+17	1.80E+17	1.65E+17
Ge-10	5.18E+17	5.22E+17	5.31E+17	5.32E+17	5.29E+17	5.20E+17	5.08E+17	4.98E+17	4.77E+17	4.56E+17

Table 5: Values of oxygen concentration from bottom to top given in atoms/cm³.

Height (mm)	4	8	12	16	20	24	28	32	36	40
Si-1	4.56E+17	4.57E+17	4.47E+17	4.47E+17	4.49E+17	4.55E+17	4.49E+17	4.59E+17	4.54E+17	4.58E+17
Ge-1	4.48E+17	4.38E+17	4.44E+17	4.34E+17	4.53E+17	4.5E+17	4.48E+17	4.49E+17	4.56E+17	4.43E+17
Ge-2	4.47E+17	4.3E+17	4.29E+17	4.6E+17	4.62E+17	4.73E+17	4.63E+17	4.25E+17	4.53E+17	4.07E+17
Ge-3	4.61E+17	4.42E+17	4.51E+17	4.74E+17	4.75E+17	4.58E+17	4.63E+17	4.79E+17	4.86E+17	4.9E+17
Ge-4	4.64E+17	4.45E+17	4.53E+17	4.71E+17	4.57E+17	4.57E+17	4.59E+17	4.55E+17	4.46E+17	4.58E+17
Ge-6	4.51E+17	4.4E+17	4.69E+17	4.69E+17	4.68E+17	4.59E+17	4.65E+17	4.6E+17	3.93E+17	//
Ge-8	4.54E+17	4.55E+17	4.54E+17	4.51E+17	4.55E+17	4.53E+17	4.56E+17	4.56E+17	4.57E+17	4.5E+17
Ge-10	4.4E+17	4.4E+17	4.41E+17	4.3E+17	4.44E+17	4.42E+17	4.42E+17	4.43E+17	4.5E+17	4.51E+17

Table 6: Values of carbon concentration from bottom to top given in atoms/cm³.

Height (mm)	4	8	12	16	20	24	28	32	36	40
Si-1	4.10E+17	4.04E+17	4.07E+17	4.09E+17	4.04E+17	3.90E+17	3.69E+17	3.47E+17	3.21E+17	3.00E+17
Hf-1	3.23E+17	3.01E+17	2.79E+17	2.60E+17	2.45E+17	2.33E+17	2.16E+17	1.90E+17	1.73E+17	//

Table 7: Values of oxygen concentration from bottom to top given in atoms/cm³.

Height (mm)	4	8	12	16	20	24	28	32	36	40
Si-1	4.56E+17	4.57E+17	4.47E+17	4.47E+17	4.49E+17	4.55E+17	4.49E+17	4.59E+17	4.54E+17	4.58E+17
Hf-1	4.23E+17	5.09E+17	5.88E+17	5.95E+17	5.59E+17	5.51E+17	5.44E+17	5.09E+17	4.44E+17	//

Table 8: Values of carbon concentration from bottom to top given in atoms/cm³.

	Height (mm)	4	8	12	16	20	24	28	32	36	40	44
Si-1	ρ (Ωcm)	1.28	1.24	1.14	1.10	1.12	0.97	1.00	0.99	0.85	0.83	0.75
Ge-10	ρ (Ωcm)	0.91	1.23	1.18	1.13	1.09	1.04	0.98	0.92	0.89	0.80	0.71
Ge-8	ρ (Ωcm)	1.21	1.11	1.15	1.07	0.98	1.04	0.85	0.90	0.87	0.78	0.69
Ge-6	ρ (Ωcm)	1.11	1.08	0.86	1.24	0.77	0.51	0.89	0.96	0.80	0.86	0.78
Ge-4	ρ (Ωcm)	1.35	1.15	1.16	1.26	1.09	1.04	0.94	0.91	0.90	0.80	0.85
Ge-1	ρ (Ωcm)	1.39	1.32	1.16	0.83	0.89	1.09	0.57	1.27	0.94	0.63	0.74
Ge-2	ρ (Ωcm)	0.82	1.03	1.05	0.90	1.05	0.83	0.93	0.99	0.77	0.59	0.65
Ge-3	ρ (Ωcm)	1.21	1.12	1.13	0.91	1.26	1.29	0.96	0.99	0.87	0.78	0.74

Table 9: Resistivity in Ge-doped samples.

	Height (mm)	4	8	12	16	20	24	28	32	36	40	44
Hf-1	ρ (Ωcm)	1.25	1.04	1.00	1.11	0.81	0.53	0.86	0.92	0.78	0.70	0.54
Hf-2	ρ (Ωcm)	0.34	0.49	0.26	0.19	0.26	0.23	0.25	0.13	0.11	0.09	0.09

Table 10: Resistivity in Hf-doped samples.

	Height (mm)	Si-1	Ge-10	Ge-8	Ge-6	Ge-4	Ge-1	Ge-2	Ge-3
Mean Linear Intercept Length (mm)		4.324	4.211	4.133	4.000	4.170	4.000	4.100	3.934

Table 11: Mean Linear Intercept Length values for Ge-doped samples.